C.P. No. 668

C.P. No. 668

MINISTRY OF AVIATION

AERONAUTICAL RESEARCH COUNCIL

CURRENT PAPERS

Aeroelastic Problems of High Speed Aircraft

by

D. Moxon

LONDON: HER MAJESTY'S STATIONERY OFFICE

1964

SEVEN SHILLINGS NET

U.D.C. No. 533.6.013.42 : 629.13.072.2

C.P. No.668

May, 1957

Aeroelastic Problems of High Speed Aircraft

by

D. Moxon

SUMMARY

Aeroelastic calculations on a number of specific aircraft projects have recently been made to provide comparative assessments. The characteristics of the aircraft were such as to provide valuable data on the aeroelastic problems of future high speed aircraft with specific reference to wing planforms and foreplane control. The flutter, divergence and aileron reversal speeds are given for the various projects and general conclusions are drawn. Throughout the work simple arbitrary modes have been assumed and simple beam theory used in evaluating the elastic stiffnesses. Approximate three-dimensional aerodynamic derivatives have been used in most of the work, and in the flutter calculations the effect of Mach No. has been estimated only by empirical rules. The value of the results is limited by these assumptions.

Replaces R.A.E. Report No. Structures 221 - A.R.C. 19 665.

LIST OF CONTENTS

LIST OF ILLUSTRATIONS

LIST OF ILLUSTRATIONS (Contd.)

1 Introduction

Five firms submitted tenders to a specification for a certain high speed aircraft. The suggested wings all had a low-aspect ratio, but the wing planforms and engine positions varied considerably. The wide variety of layouts suggested indicates that there are quite a number of aerodynamic shapes which will provide a reasonable answer to the operational requirements; but the aeroelastic characteristics differ considerably. A quantitative comparison of the wing planforms has been made with regard to flutter and aileron reversal; and curves of flutter speed against foreplane control frequency enable a qualitative comparison to be made of the foreplanes.

The five tenders are referred to throughout this paper as A, B, C, D and E. Also 'wing of aircraft D' for example is abbreviated and referred to simply as 'wing D'. All aircraft except D were of canard layout; all except E had steel as their main structural material. Throughout the work simple beam theory was used in calculating the elastic stiffnesses. Incompressible aerodynamic derivatives were used throughout the flutter calculations and the effect of Mach No. was estimated by empirical rules. In the aileron reversal calculations compressible derivatives were used although the transonic range had to be covered by interpolation of the results obtained outside this range. In view of these simplifications the results and conclusions must be regarded as tentative.

It is emphasized that the work relates to the designs as tendered, and subsequent development by the firms concerned (which in some cases has been considerable) has had to be ignored.

2 Wing flutter

The wing planforms and the assumed torsion boxes (as broken lines) are shown in fig.1. On all five tenders senary flutter calculations were made, the wings being assumed encastered at the root and deforming in simple arbitrary modes. In addition to the structural modes a body freedom mode of roll was assumed for antisymmetric flutter. In the calculating of the coefficients associated with these modes a large number of figures was retained and the high cross-inertias were then eliminated by suitable matrix transformations. Control surface flutter was investigated on each aircraft.

For wings A, B and C oscillatory derivatives were estimated from the three-dimensional incompressible static derivatives as suggested by Minhinnick[1]. On wings D and E, Woodcock's delta-wing incompressible derivatives[2] were used. On wings A and D the aerodynamic forces on the engine nacelles themselves were ignored but on the wing A their presence was assumed to increase the effective aspect ratio - and hence the magnitude of the derivatives - of the wing and control surface. On the wing D, since the delta-wing derivatives used are only strictly applicable to a wing without engine nacelles, their presence was totally ignored in evaluating the wing derivatives but, as on the wing A, they were assumed to increase the effective aspect ratio of the control surface. Stiffnesses throughout were estimated theoretically by the use of simple beam theory; control circuit stiffnesses (and hence control frequencies) were varied. Details and results of the calculations on each aircraft follow. The flutter speeds quoted are unfactored for the effect of Mach No. A possible factor is $(1-0.166\ M \cos \Lambda)$, where M is the Mach No. at the critical flutter speed and Λ is the sweepback of the leading-edge.

2.1 Aircraft A*

Wing A is constructed of steel sandwich panels. The engines are at the wing tips and with nacelles, airbrakes and outriggers weigh 32,600 lb.

* The information given in this and subsequent sections relates to the designs as they were tendered. Any subsequent development work by the firms is clearly outside the scope of the present paper.

The total wing weight (tanks full) is 69,200 lb, so that as much as 47 per cent of the weight is concentrated at the wing tips. The assumed generalised displacements of the wing-aileron system were:-

$$z\ \text{(mid-chord)} = c_r \{f_1(\eta)q_1 + f_2(\eta)q_2 + f_3(\eta)q_3\}$$

$$\alpha = f_4(\eta)q_4 + f_5(\eta)q_5$$

$$\beta = q_6$$

where $\eta = {}^y/s$, a non-dimensional spanwise variable

α is line-of-flight incidence of wing

and $f_1 = \eta$ (the rolling freedom)

$$\left.\begin{array}{l} f_2 = \eta^2 \\ f_3 = \eta^3 \end{array}\right\} \text{coupled frequencies, 1.5 and 10 c.p.s.}$$

$$\left.\begin{array}{l} f_4 = \eta \\ f_5 = \eta^2 \end{array}\right\} \text{coupled frequencies, 2.9 and 6.8 c.p.s.}$$

Each overtone mode (the 10 c.p.s. and 6.8 c.p.s.) had a node near the wing tip.

The calculations indicate that the wing has a symmetric divergence speed of 700 knots and an antisymmetric flutter speed of 563 knots. The flutter frequency is 4.68 c.p.s., some 70% of the overtone torsion frequency associated with the two arbitrary torsion modes. The frequency parameter is 0.96; and this high value, it would seem, is a result of overtone flutter, that is, flutter in which an overtone mode is essential. Aileron rotation is destabilizing; for example, the flutter speed falls to 490 knots for an aileron rotation frequency of 10 c.p.s. A point of interest in the investigation was the stiffness effect of the engine thrust. This was allowed for by the introduction of bending stiffnesses into the torsion modes (cross-stiffnesses) and led to an asymmetric stiffness matrix. The size of the elements of this matrix and the structural stiffness matrix are set out below for comparison. The structural stiffness matrix for modes 1 to 5 is:-

$$\begin{array}{ccccc} 0 & 0 & 0 & 0 & 0 \\ 0 & 53 & 58 & 0 & 0 \\ 0 & 58 & 83 & 0 & 0 \\ 0 & 0 & 0 & 10.3 & 8.1 \\ 0 & 0 & 0 & 8.1 & 8.2 \end{array}$$

The elements of the "engine-thrust" stiffness matrix are all zero except E_{14}, E_{15}, E_{24}, E_{25}, E_{34} and E_{35} all of which are of magnitude 1.31. The effect on the flutter speed of including these stiffness contributions was found to be very small. In subsequent calculations on the other tenders these stiffness contributions from the engines were neglected.

2.2 Aircraft B

The wing structure is basically a tapered Warren-girder continuum, the upper and lower wing surfaces being steel sandwich panels. The wing has no aileron: roll is produced by differential rotation of the foreplane. At the wing tips subsonic drop-tanks are attached; jettison occurs at a Mach No. of 0.9 at 36,000 ft (280 E.A.S.). In spite of the specified early (low E.A.S.) jettison the drop-tanks-on (and full) loading case was investigated. In particular the investigation was directed at finding whether some prohibitive tank attachment frequency would be needed to avoid flutter.

The wing-tank combination was assumed to deform in six arbitrary modes; aircraft roll, two wing distortion modes, drop-tank rotation (roll) and two drop-tank distortion modes. If z_w and α_w are the vertical displacement and aerodynamic incidence of the wing in the wing modes, and z_t and α_t the vertical displacement and aerodynamic incidence at the tank in the tank modes; then the assumed displacements are given by

$$z_w \text{ (wing mid-chord)} = c_r \{f_1(\eta_w)q_1 + f_2(\eta_w)q_2\}$$

$$\alpha_w = f_3(\eta_w)q_3$$

$$z_t \text{ (tank mid-chord)} = c_r \{f_4(\eta_t)q_4 + f_5(\eta_t)q_5\}$$

$$\alpha_t = f_6(\eta_t)q_6$$

where $\eta_w = {}^{y_w}/s$, y_w measured from aircraft centre line

$\eta_t = {}^{y_t}/s$, y_t measured outwards from wing tip

and $f_1 = \eta_w$ (aircraft roll)

$f_2 = \eta_w^2$ with an uncoupled frequency of 3.69 c.p.s.

$f_3 = \eta_w$ with an uncoupled frequency of 13.4 c.p.s.

$f_4 = \eta_t$ frequency varied

$f_5 = \eta_t^2$ with an uncoupled frequency of 14.9 c.p.s.

$f_6 = \eta_t$ with an uncoupled frequency of 14.4 c.p.s.

In addition to the displacements listed above there are of course, rigid body displacements of the drop-tanks in the wing modes.

The results indicate that the critical speeds obtained for the 23 binary and the 123 ternary are much the same as those obtained when the tank flexibilities - as expressed in modes 4 and 6* - were included. The actual results are tabulated below.

Modes	Frequency of mode 4 - c.p.s.	Critical condition	Critical speed - knots	Frequency - c.p.s.
23	-	flutter	1184	7.5
123	-	flutter	1176	7.7
236	-	divergence	1198	-
12346	3 - ∞	flutter	1100 (approx.)	6.5 (approx.)

* Mode 5 was ignored throughout since the inertia and aerodynamic coefficients in it and mode 4 were very similar.

It appears that the drop-tanks and their attachment are not likely to prove a serious aeroelastic problem: calculations indicate that a high attachment frequency is not required in the rolling freedom; and, if it is required in the pitching freedom, it should not prove difficult to provide.

A flexure-torsion binary calculation indicated that the bare wing is free from flutter at all airspeeds but diverges at 1770 knots.

2.3 Aircraft C

This low aspect-ratio delta wing with a leading-edge sweep of 70° is of steel sandwich construction. In front of the torsion box there is a large cut-out to form a wheel well (see fig.1). The engines are distributed spanwise inboard of the aileron and close to the trailing-edge.

Assessment of this wing proved difficult: low aspect-ratio and high leading-edge sweep were largely responsible for this. To make any assessment at all in the very limited time available, simple modes involving no chordwise bending had to be assumed and simple beam theory was used in calculating the elastic stiffness coefficients. Three-dimensional static aerodynamic derivatives were quoted in the brochure and these were used in estimating the oscillatory derivatives.

The wing was assumed to deform in six arbitrary modes; aircraft roll, four structural distortion modes and aileron rotation. The wing was assumed to twist about a line 14.83 ft in front of the trailing-edge. The vertical displacement (z) of this line was given by

$$z = c_r \{f_1(\eta)q_1 + f_2(\eta)q_2 + f_3(\eta)q_3\} .$$

Also

$$\alpha = f_4(\eta)q_4 + f_5(\eta)q_5$$

$$\beta = q_6$$

where α is the line-of-flight incidence of the wing

and $f_1 = \eta$

$$\left.\begin{aligned} f_2 &= \eta^2 \\ f_3 &= \eta^3 \end{aligned}\right\} \text{fundamental bending frequency 6.3 c.p.s.}$$

$$\left.\begin{aligned} f_4 &= \eta^2 \\ f_5 &= \eta^3 \end{aligned}\right\} \text{fundamental torsion frequency 9.9 c.p.s.}$$

Elastic stiffness contributions in the torsion modes were assumed to come from the torsion box and the wing in front of the wheel well: the torsion box was assumed to resist twisting and bending but the front part of the wing bending only. The locus of shear centres of the torsion box was assumed to be a constant distance in front of the trailing-edge and coincident with the torsion box mid-chord line over the inboard part. The skin thicknesses (in steel) assumed were: for the torsion box, 0.036 in. in torsion and 0.046 in. in bending; and for the front part of the wing 0.030 in. The results of the flutter calculation show two forms of flutter, similar to those obtained on aircraft D and discussed in the next section, which are distinguished by a high frequency when the aileron frequency is low and a low frequency at high aileron frequencies. The aileron has very little effect on flutter speed while its frequency is greater than 20 c.p.s.; for aileron frequencies less than this, the flutter speed falls rapidly as the aileron frequency is reduced. The flutter speeds and frequencies obtained are tabulated below.

Aileron frequency - c.p.s.	Symmetric flutter speed - knots	Symmetric flutter frequency - c.p.s.	Antisymmetric flutter speed - knots	Antisymmetric flutter frequency - c.p.s.
∞	1923	7.5	2085	3.2
10	1506*	15.9	984	11.0

The effect of neglecting all the stiffness contributions from the front part of the wing was investigated. Their neglect resulted in an unrealistic ratio of the fundamental flexural frequency to the fundamental torsion frequency so that the result obtained, which was in fact divergence at 1440 knots, may be misleading.

Clearly the results obtained for this wing cannot be expected to be numerically accurate, but it is thought that the high values of the basic wing critical speeds are such that the main wing structure is at least adequate for the avoidance of flutter and divergence.

2.4 Aircraft D

This wing is of steel multi-web construction and has a cut-out in the sheet steel skin inboard of the engines where the undercarriage retracts. Some allowance was made for this in estimating the efficiency of the skin over this section. As stated previously, wing derivatives used were those of Woodcock; for aileron and horn factored two-dimensional derivatives were used. In view of the large horn it was decided to allow the horn a separate degree of freedom - rotation of the horn about the aileron hinge line against a variable elastic constraint.

In addition to modes of aileron and horn rotation four structural distortion modes were assumed, the vertical displacement (z) of a line 27.6 ft aft of the wing apex and perpendicular to the aircraft centre-line being given by

$$z = c_r \{f_1(\eta) q_1 + f_2(\eta) q_2\} .$$

Also

$$\alpha = f_3(\eta) q_3 + f_4(\eta) q_4$$

$$\beta_{aileron} = q_5$$

$$\beta_{horn} = q_6$$

* This is, in fact, not strictly true; there is a different type of flutter below this at 1084 knots, but, since this is absent at all aileron frequencies greater than 10.2 c.p.s., it would be misleading to quote this speed to indicate the magnitude of the destabilizing effect of the aileron.

where α is line-of-flight incidence of wing

$$\left.\begin{aligned} f_1 &= \eta^2 \\ f_2 &= \eta^3 \end{aligned}\right\} \text{ fundamental frequency 2.0 c.p.s.; overtone, 9.0 c.p.s.}$$

and

$$\left.\begin{aligned} f_3 &= \eta^2 \\ f_4 &= \eta^3 \end{aligned}\right\} \text{ fundamental frequency 3.1 c.p.s.; overtone, 8.4 c.p.s.}$$

Each overtone mode had a node near the engine.

The result indicates that the wing symmetric critical speed is flutter at 627 knots at a frequency of 6.76 c.p.s. This corresponds to a frequency parameter of 0.80. The frequency of the flutter suggests some overtone mode is important. As on aircraft A, suspected overtone flutter is characterised by a high frequency parameter. Curves of flutter speed plotted against aileron frequency are given in fig.2. It will be seen that the horn frequency does not have a very marked effect on flutter speed. This result, however, must be regarded as tentative in view of the aerodynamic assumptions.

2.5 Aircraft E

This wing is constructed of an aluminium alloy skin supported by stringers, webs and ribs. Fins are carried at the wing tips and lie above the plane of the wing. The engines are distributed spanwise inboard of the ailerons.

Six arbitrary modes were assumed; aircraft roll, four structural distortion modes and aileron rotation. The wing was assumed to twist about a line 13.7 ft in front of the trailing-edge. The vertical displacement (z) along this line was given by

$$z = c_r \{f_1(\eta)q_1 + f_2(\eta)q_2 + f_3(\eta)q_3\} .$$

Also

$$\alpha = f_4(\eta)q_4 + f_5(\eta)q_5$$

$$\beta = q_6$$

where α is the line-of-flight incidence of the wing

and $f_1 = \eta$

$$\left.\begin{aligned} f_2 &= \eta^2 \\ f_3 &= \eta^3 \end{aligned}\right\} \text{ fundamental frequency 2.6 c.p.s.; overtone, 7.2 c.p.s.}$$

$$\left.\begin{aligned} f_4 &= \eta^2 \\ f_5 &= \eta^3 \end{aligned}\right\} \text{ fundamental frequency 4.3 c.p.s.; overtone, 7.5 c.p.s.}$$

Oscillatory derivatives for the fin and aileron were based on three-dimensional static; Woodcock's derivatives were used for the wing. Flutter speeds are tabulated below.

Aileron frequency - c.p.s.	Symmetric flutter speed - knots	Symmetric flutter frequency - c.p.s.	Antisymmetric flutter speed - knots	Antisymmetric flutter frequency - c.p.s.
∞	660	3.45	700	3.46
10	626	3.89	-	-

3 Comparison of the wing planforms on the basis of flutter

Aircraft A, C, D and E have roughly the same design weight and so, in a sense, the wings of these four aircraft do the same job. On the basis of the foregoing results the merits of the planforms have been assessed from an aeroelastic standpoint. To isolate the effect of planform, variables from tender to tender such as thickness/chord ratio and skin thickness were eliminated by scaling the actual wing flutter speeds to correspond to a standard value of thickness/chord ratio and skin thickness. The differences in the scaled flutter speeds is assumed to result from the differences in planform and associated layout. As a further extension a flutter speed per unit skin mass can be obtained for each layout by dividing the scaled flutter speeds by the respective wing areas*. Aircraft B, by virtue of its different design weight and different form of wing construction stands apart from the rest and does not lend itself to this type of comparison. Wing E, unlike the others, is constructed in aluminium alloy. In order to compare this planform with the rest it was assumed that the flutter speed obtained for the alloy wing would also be the flutter speed of a geometrically similar wing (apart from the thickness of the skin) of the same torsional stiffness but constructed in steel.

The flutter speeds, skin thicknesses, thickness/chord ratios etc. for the four wings are given below. The flutter speeds are then scaled to the same skin thickness and thickness/chord ratio, that for the wing A being taken as the standard. For this purpose, the flutter speeds are assumed proportional to the thickness/chord ratio** and to the square root of the skin thickness. These scaled flutter speeds, if divided by the respective wing areas, indicate the efficiency with which the skin material is used in each planform. These "planform-efficiency factors", relative to that of planform A, are given below. It will be seen that planform C is by far the most efficient and that there is little to choose between planforms A, D and E. These factors would probably be substantially the same for any sized planforms geometrically similar to the above, provided that the relative planform sizes remained the same. If the compressibility factor $1 - 0.166\, M \cos \Lambda$ (M is Mach No. at flutter, Λ is leading-edge sweep) is applied to the flutter speeds based on incompressible derivatives, all the efficiency factors are unchanged except that of the planform C which becomes 2.58.

The ratio of flutter speed when the aileron frequency is 10 c.p.s. to the wing flutter speed is quoted to give an indication of the destabilizing effect of the aileron. On wings C and D however, the type of flutter is different when the aileron frequency is 10 c.p.s. to that when it is infinite. There is a sharp discontinuity in the curves of flutter speed against

* This is not strictly true since the torsion boxes cover only part of the wing areas and elsewhere the skin is probably thinner.

** The thickness/chord ratio of wing D varied from 3.5% at the root to 3% at the tip. For the purpose of scaling the flutter speed of this wing an effective thickness/chord ratio was estimated using the strain energy in a linear torsion mode as a criterion; the estimated value was 3.37%.

aileron frequency when the type of flutter changes, and for this reason the figures quoted for wings C and D are sensitive to the reference frequency which is chosen for the aileron.

Item	Wing A	Wing C	Wing D	Wing E
Wing flutter speed (knots)	563	1923	627	660
Flutter frequency (c.p.s.)	4.68	7.50	6.76	3.45
Frequency parameter at 0.7 semi-span	0.96	0.37	0.80	0.48
Thickness/chord ratio (%)	3	4	3.5 - 3.0	4
Skin thickness in torsion (ft)	0.004,16	0.003,00	0.004,19	0.013,92
Skin material	steel	steel	steel	Al. alloy
Net area of wing (ft^2)	1714	1906	1738	1640
Flutter speed appropriate to a thickness/chord ratio of 3% and a skin thickness of 0.004,16 ft in steel	563	1698	594	520
Flutter speed per unit area, relative to wing A	1	2.71	0.97	0.97
$\frac{\text{Flutter speed, aileron frequency 10 c.p.s.}}{\text{Flutter speed, aileron frequency } \infty}$	0.87	0.51	0.89	0.95

4 Aileron reversal

Aileron reversal calculations were made on aircraft A, C and E. The semi-rigid approach was adopted, simple modes of flexure and torsion being assumed. The minimum skin thickness required to achieve an equivalent air-speed 15% in excess of the design diving speed without reversal was estimated over the specified design Mach No. range of each aircraft. A curve of skin thickness required against Mach No. for a constant E.A.S. (= 1.15 V_D) is plotted. When appropriate to a thin unswept wing, this curve has a maximum near to a Mach number of 1; and, if this maximum value of skin thickness is provided on the aircraft, it will have adequate rolling power at all speeds and Mach Nos. in its design range. The reason for plotting a curve is that it affords a visual means of interpolating the results in the critical transonic speed range, where the aerodynamic derivatives are uncertain. Just below a Mach number of 1 - still considering thin unswept wings - the lift due to control surface rotation begins to move back from about the half chord to the mid-aileron chord, and at roughly the same Mach No. the wing aerodynamic centre begins to move from the region of the quarter chord to the half chord. It is these movements, in particular the relative positions of the centre of pressure due to increments of wing incidence and aileron angle, that largely determine the reversal speed. The worst possible case occurs when the aileron lift has moved back and the wing centre-of-lift is still forward.

All the aerodynamic derivatives obtained for the wing-aileron systems were overall derivatives, whereas strip derivatives were required for the calculations. To convert the overall derivatives to the strip derivatives necessitated an assumption for the spanwise lift distribution; the assumed distributions are quoted for each aircraft under the appropriate heading. The derivatives involved are:

$$\frac{\partial C_L}{\partial \alpha} \; (= a_1) \; , \quad \frac{\partial C_M}{\partial \alpha} \; , \quad \frac{\partial C_L}{\partial \beta} \; (= a_2) \; , \quad \frac{\partial C_M}{\partial \beta} \; .$$

These derivatives define the magnitude and position of lift due to wing incidence and aileron angle. Details and results for each aircraft follow.

4.1 Aircraft A

Modes of linear and parabolic torsion about the mid-chord line were assumed; flexure modes were neglected owing to the lack of appreciable sweep. The lift due to wing incidence and lift due to aileron angle were assumed to act at a constant fraction of the local chord; the spanwise distribution of the lifts was assumed proportional to the chord (i.e. constant a_1 and a_2), the aileron-induced lift extending over the aileron span only. These assumptions are appropriate to two-dimensional aerodynamics since the aileron chord is a constant fraction of the wing chord. Curves of skin thickness against Mach No. for an equivalent airspeed of 559 knots are given in fig.3. The points on the curve at subsonic and supersonic speeds were calculated, but between Mach Nos. of 0.9 and 1.5 the broken-line curve is an interpolation. The effect of including the rolling moment due to the deflected engine thrust line at reversal was investigated and found to be small (see fig.3).

The design diving speed of this aircraft is 486 knots E.A.S. at sea-level, 450 at 26,000 ft and 475 at 60,000 ft. A speed of 486 knots at sea-level corresponds to a Mach No. of 0.73; and the skin thickness required at this Mach No. (at sea-level) can be read from the graph directly as 45 thousandths of an inch. Also a speed of 486 knots E.A.S. and a Mach No. of 1 would call for a skin thickness of 71 thou; but the aircraft is never required to fly at 486 knots E.A.S. when the Mach No. is 1. In fact, if the design diving speed varies linearly with altitude up to 26,000 ft, the design diving speed has dropped to 460 knots E.A.S. by the time the aircraft is flying at the speed of sound. This condition was found to be the most adverse; and the skin thickness requirement is obtained by multiplying the skin thickness of 71 thou. by $\left(\frac{460}{486}\right)^2$, giving 64 thou. For the sake of comparison the skin thickness required to achieve a wing flutter speed of 1.25 V_D at sea-level is indicated; both the factored (for compressibility) and unfactored results are represented.

4.2 Aircraft C

Low aspect ratio and high leading-edge sweep combined to make even a preliminary assessment of this wing difficult. Only supersonic derivatives could be obtained, and shortage of time precluded the use of any but simple beam theory for calculating the elastic stiffness coefficients, which were the same as those used in the wing flutter calculations (see section 2.3). Overall derivatives being quoted for the aileron, the actual aileron was replaced by a rectangular aileron of the same span as the original and the same chord as the inner part. The lift due to aileron was assumed constant along the aileron span (the investigation was restricted to supersonic speeds) and acting at a constant fraction of the aileron chord the magnitude and position being such as to give the same overall lift and pitching moment as estimated for the original. Over the wing the spanwise load distribution was assumed to be elliptic and the locus of aerodynamic centres was assumed to be a straight line at a constant fraction of the chord. Modes of parabolic and cubic torsion about an axis 14.83 ft in front of the trailing edge and parabolic flexure were considered. A curve of required skin thickness against Mach No. for an equivalent airspeed of 805 knots is given in fig.4. The design diving speed of this aircraft is 700 knots E.A.S. from sea-level up to 45,000 ft; above 45,000 ft the restriction is M = 2.75. All points on the curve are realistic in that they correspond to altitudes less than 45,000 ft.

4.3 Aircraft E

This wing is constructed in dural whereas the other two are in steel. As on aircraft C the investigation was restricted to the supersonic speed range as derivatives at other Mach Nos. could not be obtained. The locus of aerodynamic centres was assumed to be a straight line at a constant fraction of the chord, and the spanwise load distribution was assumed to be the mean of an elliptic distribution and a distribution proportional to the chord. Lift due to aileron was taken to act at a constant fraction of the aileron chord aft of the hinge line. A curve of skin thickness against Mach No. for an airspeed of 595.7 knots is given in fig.5.

The design diving speed of this aircraft is 518 knots E.A.S. from sea-level to 36,000 ft and 484 knots at 57,000 ft. For an E.A.S. restriction of 518 knots, Mach Nos. up to 1.65 can be achieved below 36,000 ft; the curve to the left of the vertical intercepting line thus corresponds to actual flight conditions. The effect of the decrease in design E.A.S. above 36,000 ft is to lessen the skin requirements predicted by the right-hand portion of the curve.

5 Comparison of the wing planforms on the basis of aileron reversal

In figs.3, 4 and 5 the skin thickness required on each aircraft to achieve 1.15 V_D was given. Owing to differences in each design, of which material of construction, thickness/chord ratio and design diving speed are perhaps the most important, any comparison as to the best planform based directly on these graphs would be unrealistic. To effect a truer comparison each graph was rescaled to correspond to a 4% thick wing of steel construction and an aileron reversal speed of 600 knots E.A.S.; the result is shown in fig.6.

6 Foreplane flutter

Four of the five tenders submitted were of canard layout, the exception being aircraft D. Calculations were made on all the canard layouts. The assumed foreplane shapes are shown in fig.7, the aircraft centre-lines and foreplane pitching axes being shown as chain-dotted lines. The flutter calculations made involved structural modes of fuselage flexure and torsion, and foreplane flexure and torsion. The associated structural stiffnesses were based on the skin thicknesses quoted or calculated from the overall weight. Other modes were foreplane rotation, elevator rotation and elevator torsion; in such modes the frequencies were left as variables. These frequencies do, in fact, to a large extent remain unknown until detailed calculations and measurements have been made on the prototype aircraft; in any case they could probably be modified - within limits - without an appreciable increase in overall weight. These preliminary calculations were intended to indicate what order of control frequencies are needed to attain the required V_D.

Symmetric and antisymmetric arbitrary mode calculations were made on all aircraft but one, the exception being aircraft E on which no anti-symmetric calculations were made because of the high degree of taper of both foreplane and elevator. In the symmetric flutter calculations the fuselage modes envisaged were fundamental and overtone flexure and in the anti-symmetric, fundamental and overtone torsion. Since the assumed fuselage modes were similar for each aircraft, it is convenient to express the modal displacements and rotations in general terms and then particularise for each aircraft.

In the arbitrary mode symmetric flutter calculations the displacement (z) of the fuselage in the two fuselage modes was given by

$$\text{Mode 1:} \quad z = c_r \xi^2 q_1$$

$$\text{Mode 2:} \quad z = c_r \xi^2 (1-k\xi) q_2$$

where ξ is distance (non-dimensionalised) of any point in fuselage in front of the fuselage node in mode 1

$\bar{\xi}$ is distance (non-dimensionalised) of any point in fuselage in front of the fuselage node in mode 2

k is such that $A_{12} = 0$.

$\xi = 0$ and $\bar{\xi} = 0$, the fixing points in modes 1 and 2, were judged roughly from the mass distribution.

In the arbitrary mode antisymmetric calculations the rotation (θ) of any section was given by

$$\text{Mode 1:} \quad \theta = \xi q_1$$

$$\text{Mode 2:} \quad \theta = \bar{\xi}(1-k\bar{\xi})q_2$$

where ξ, $\bar{\xi}$ and k have the same meanings as above.

In addition to this arbitrary mode approach, calculations involving fuselage calculated normal modes were made on aircraft A and E. These 'normal' modes were obtained by making the arbitrary symmetric modes orthogonal with respect to pitch, vertical translation and each other. The first step was to eliminate the cross inertial coupling between the fuselage structural modes and the body freedom modes by a matrix transformation. Since the elastic stiffnesses associated with the body freedom modes were already zero, the four original modes had now been reduced to: two modes of zero frequency and zero inertial and elastic coupling, and two other modes both orthogonal to pitch and vertical translation. These latter pair provided the 'normal' modes.

Throughout the work, oscillatory aerodynamic derivatives for the foreplane were based on three dimensional incompressible static derivatives as suggested by Minhinnick. In some cases account was taken of the aerodynamic forces on the fuselage by the use of slender body theory. Details of calculations on each aircraft follow. Calculations involving the types of fuselage modes described above are, for convenience, referred to as arbitrary symmetric, arbitrary antisymmetric and 'normal' symmetric. The flutter speeds quoted do not include the Mach No. correction. The effect of compressibility can be estimated by multiplying the flutter speed based on incompressible flow by $1-0.166\ M\cos\Lambda$, as in the wing flutter calculations.

6.1 Aircraft A

This design was probably investigated the most extensively; flutter involving each type of fuselage mode was considered. The nodal point in mode 1 was assumed to be at the wing apex, which is 58 ft aft of the foreplane hinge line; in mode 2, 16 ft aft of the apex. The calculated frequencies of the fuselage modes are given below.

Arbitrary symmetric modes: uncoupled frequencies, 3.4 and 12 c.p.s.; coupled, 2.9 and 12.1 c.p.s.

Arbitrary antisymmetric modes: uncoupled frequencies, 16 and 44 c.p.s.

'Normal' symmetric modes: frequencies 6 and 13 c.p.s.

The assumed foreplane modes were:-

Mode 3 Parabolic flexure of foreplane at an uncoupled frequency of 9.8 c.p.s.

$$z = c_r \eta^2 q_3$$

$$\alpha = 0 .$$

Mode 4 Rotation of foreplane about its hinge line - frequency varied

$$z = c_r \xi_1 q_4$$

$$\alpha = q_4 .$$

Mode 5 Torsion of foreplane about mid-chord at an uncoupled frequency of 20.2 c.p.s.

$$z = c_r \eta \xi_2 q_5$$

$$\alpha = \eta q_5 .$$

Mode 6 Elevator rotation - frequency varied

$$z = c_r \xi_3 q_6$$

$$\beta = q_6$$

where η is a non-dimensional spanwise variable, $\eta = 0$ on a/c centre line

ξ_1 " " " " chordwise " , $\xi_1 = 0$ on foreplane hinge line

ξ_2 " " " " " " , $\xi_2 = 0$ on foreplane mid-chord

ξ_3 " " " " " " , $\xi_3 = 0$ on elevator hinge line

No allowance was made for the aerodynamic forces on the fuselage.

Curves of flutter speed against foreplane rotation for the arbitrary symmetric and 'normal' symmetric calculations are given in fig.8. At low foreplane rotation frequencies (<10 c.p.s.) the flutter is essentially binary flutter between fundamental fuselage flexure and foreplane rotation. At high rotation frequencies the flutter tends to ternary flutter involving foreplane flexure, torsion and rotation; flexure-torsion flutter itself is absent below 2,372 ft/sec. A large difference will be observed in the senary results for the arbitrary and 'normal' mode calculations. In view of the similarity of the quinary results it would appear that the fundamental fuselage mode is largely responsible for this. In the arbitrary mode calculations the fundamental mode at 3.4 c.p.s. stabilized the flutter obtained for the quinary and led to divergence at an airspeed of about 1780 ft/sec. In the 'normal' mode calculations, the fundamental mode at 6 c.p.s. had the effect of displacing the quinary curve to the right. This difference in effect was not due only to the difference in frequencies of the two modes: e_{11} in the arbitrary mode calculations was adjusted to give a fundamental frequency of 6 c.p.s. and the resulting curve of flutter speed against foreplane rotation frequency did not agree even roughly with the 'normal' mode curve.

Curves of antisymmetric flutter speed against foreplane rotation frequency are given in fig.10. As the fuselage frequencies are increased the right hand part of the curves - where the foreplane torsion and rotation are greater than the foreplane bending frequency - are lowered. The effect of the fuselage torsion modes, particularly the fundamental, is probably to modify the foreplane flexure mode, the fundamental mode of this combination coupling with foreplane torsion and rotation to give flutter. A frequency increase in the fuselage torsion modes results in an increase in the frequency of the fundamental flexure mode; this approach to the foreplane torsion and rotation frequencies results in a decrease in flutter speed.

Curves of flutter speed against the elevator rotation frequency for the arbitrary symmetric and 'normal' symmetric calculations are given in fig.9; corresponding curves for the arbitrary antisymmetric calculations are given in fig.11.

6.2 Aircraft B

Arbitrary mode calculations only were made on this aircraft, although both symmetric and antisymmetric flutter were considered. The fuselage fixing points in modes 1 and 2 were assumed to be 38.6 ft aft of the foreplane hinge line. The frequencies of the fuselage modes are given below.

Arbitrary symmetric modes: uncoupled frequencies, 3.1 and 11.4 c.p.s.

Arbitrary antisymmetric mode: uncoupled frequency, 8.7 c.p.s.

The overtone antisymmetric fuselage mode was neglected.

The assumed modes of the foreplane were:-

Mode 3 Parabolic bending along hinge line at an uncoupled frequency of 10.1 c.p.s.

$$z = c_r \eta^2 q_3 + \alpha(c_r \xi_1)$$

$$\alpha = \frac{c_r}{s} \eta \sin 2\Lambda_1 \; q_3 \; .$$

Mode 4 Foreplane rotation about hinge line - frequency varied

$$z = c_r \xi_1 \cos \Lambda_1 \; q_4$$

$$\alpha = \cos \Lambda_1 \; q_4 \; .$$

Mode 5 Foreplane linear torsion about mid-chord at an uncoupled frequency of 23.3 c.p.s.

$$z = c_r \eta \xi_2 \cos \Lambda_2 \; q_5$$

$$\alpha = \cos \Lambda_2 \; q_5$$

where α is the line-of-flight incidence of foreplane

Λ_1 is the sweepback of the hinge line

Λ_2 is the sweepback of the mid-chord line.

The other symbols have the same meaning as they had in section 6.1. No allowance was made for the aerodynamic forces on the nose.

Curves of flutter speed against foreplane rotation frequency for the symmetric and antisymmetric cases are given in figs. 12 and 13 respectively. The symmetric flutter is insensitive to variations in the fuselage frequencies; this is particularly so at high foreplane rotation frequencies. Here the flutter is flexure-torsion flutter of the foreplane modified to a small extent by the foreplane rotation mode. This modification leads to an 8% drop in flutter speed when the foreplane rotation frequency is 40 c.p.s. The antisymmetric flutter speed is more sensitive to variations in fuselage stiffness than the symmetric. The flutter speed decreases as the fuselage torsional stiffness is increased as on foreplane A. It is of interest to note that symmetric flutter occurs at lower airspeed than antisymmetric flutter when the foreplane rotation frequency is between 14 and 40 c.p.s.

6.3 Aircraft C

The foreplane of this aircraft is essentially different from the others. Two features peculiar to it are its highly swept delta configuration and its having foreplane and elevator axes coincident. The node in the fuselage modes was assumed to be 57.5 ft aft of the hinge line. Its symmetric and antisymmetric flutter characteristics were investigated using arbitrary modes. The calculated frequencies of the fuselage modes were:-

Arbitrary symmetric modes: uncoupled frequencies, 3.6 and 15.9 c.p.s.

Arbitrary antisymmetric mode: frequency of fundamental 18.9 c.p.s.

The foreplane modes were:-

Mode 3 Parabolic bending of foreplane at an uncoupled frequency of 15.7 c.p.s.

$$z = c_r \eta^2 q_3$$

$$\alpha = 0 .$$

Mode 4 Rotation of foreplane about its hinge - frequency varied

$$z = c_r \xi_1 q_4$$

$$\alpha = q_4 .$$

Mode 5 Linear torsion of elevator - frequency varied

$$z = c_r \eta \xi_2 q_5$$

$$\alpha = \eta q_5 .$$

Mode 6 Rotation of elevator - frequency varied

$$z = c_r \xi_3 q_6$$

$$\beta = q_6$$

where symbols have the same meaning as they had in section 6.1.

The foreplane torsion mode has been omitted as it would be a very high frequency mode and unlikely to play any significant part in flutter in the speed range under consideration. Fuselage aerodynamics were based on results obtained on aircraft E.

The results obtained for aircraft C were quite different from the results obtained on the other three. At elevator torsion and rotation frequencies of 25 and 30 c.p.s. all symmetric flutter below 1500 ft/sec was confined to foreplane rotation frequencies between 13.4 and 17.6 c.p.s. Antisymmetric flutter was absent below 2200 ft/sec at all foreplane rotation frequencies. By decreasing the elevator torsion frequency sufficiently the extent of the flutter, both symmetric and antisymmetric, was increased. Curves of flutter speed against foreplane rotation at such a torsional frequency are given in fig. 14. The stabilizing effect of the fuselage torsion mode, observed on aircraft A and B, is seen in this case to be very marked. The effect of the elevator torsion frequency on flutter was investigated for the particular case of a high foreplane rotation frequency; the results are shown in fig. 16. It is seen that the flutter is basically foreplane bending-elevator torsion flutter, and flutter can be eliminated by increasing the torsion stiffness of the elevator provided the elevator rotation frequency is sufficiently high, e.g. 25 c.p.s. For an elevator rotation frequency of 10 c.p.s., the flutter is not eliminated: as the torsion frequency is increased foreplane bending-elevator torsion flutter gives way to foreplane bending-elevator rotation flutter.

6.4 Aircraft E

Arbitrary and 'normal' symmetric calculations were made on this aircraft. The fixed points in the fuselage were assumed to be 51 ft aft of the foreplane hinge line. The calculated frequencies of the fuselage modes are given below.

Arbitrary symmetric modes: uncoupled frequencies 5.0 and 20.1 c.p.s.

'Normal' symmetric modes: frequencies 7.4 and 24.6 c.p.s.

The assumed foreplane modes were:-

Mode 3 Parabolic bending at an uncoupled frequency of 9.0 c.p.s.

$$z = c_r \eta^2 q_3$$

$$\alpha = 0 .$$

Mode 4 Rotation of foreplane about its hinge line - frequency varied

$$z = c_r \xi_1 q_4$$

$$\alpha = q_4 .$$

Mode 5 Linear torsion of foreplane about mid-chord at 30.1 c.p.s.

$$z = c_r \eta \xi_2 q_5$$

$$\alpha = q_5 .$$

Mode 6 Rotation of elevator - frequency varied

$$z = c_r \xi_3 q_6$$

$$\beta = q_6$$

where symbols have the same meaning as they had in section 6.1.

Account was taken of the aerodynamic forces acting on the fuselage nose but they were found to have no appreciable effect.

Curves of flutter speed against foreplane rotation frequency are given in fig.17, both for the 'normal' and arbitrary modes. It will be seen that the curves are still rising quite steeply at foreplane rotation frequencies between 20 and 30 c.p.s. This is presumably because the flexure-torsion binary flutter speed - to which the curves in fig.17 will be roughly asymptotic - is high. This high binary flutter speed (3060 ft/sec) results mainly from a high torsional stiffness and a high degree of taper. Curves of flutter speed against elevator rotation frequency are given in fig.18.

7 Concluding remarks on foreplane flutter

The following observations are made on the foreplane flutter calculations.

(i) Results obtained from symmetric flutter calculations differ widely according to whether the fuselage modes are orthogonal with respect to the body freedoms or not. We may conclude that in arbitrary mode foreplane calculations the body freedoms pitch and vertical translation should either be incorporated in the fuselage modes or included as separate degrees of freedom.

(ii) An increase in fuselage torsion stiffness results in a decrease in flutter speed when the foreplane rotation frequency is above and away from the foreplane bending frequency and the elevator rotation frequency is high. A similar destabilizing effect would be expected in elevator flutter and this is, in fact, confirmed at isolated elevator frequencies. Symmetric flutter involving primarily foreplane flexure, rotation and torsion is less sensitive to changes in fuselage stiffness.

(iii) On aircraft A, B and C, the symmetric flutter speed is lower than the antisymmetric when the foreplane rotation frequency is above and away from the foreplane bending frequency and the elevator rotation frequency is high. This arises partly as a result of the stabilzing effect of the fuselage torsion mode mentioned in (ii). No antisymmetric calculations were done on aircraft E and so no comparison is possible.

(iv) In foreplane flutter in which the elevator plays no significant part, the higher the flexure-torsion flutter speed, the lower, in general, is the foreplane rotation frequency that is necessary to achieve a certain V_D.

(v) The possibility of divergence is real if the foreplane control stiffness is low.

8 Fin flutter

Calculations were made on aircraft A, C and E; the assumed shapes are shown in fig.19. The fins on aircraft A and C are placed centrally but the fins on aircraft E are at the wing tips. Throughout the work, factored two dimensional incompressible derivatives were used in calculating the aerodynamic coefficients. The factors applied were $\cos \Lambda \{f(A)\}^2$ to the stiffness derivatives and $\cos\Lambda\, f(A)$ to the damping derivatives (Λ is sweep of leading-edge and $f(A) = 1 + 0.8/A_E$, where A_E is the effective aspect ratio of fin in position on the aircraft). Details of the calculations and results obtained on each aircraft follow. The flutter speeds quoted do not include the Mach No. correction. The effect of compressibility may be estimated in the same way as for the wing and foreplane flutter calculations.

8.1 Aircraft A

The fin was assumed to be encastered at the root and to deform in modes of parabolic bending, parabolic and cubic torsion and rudder rotation. i.e.

$$z = c_r f_1(\eta) q_1$$

$$\alpha = f_2(\eta) q_2 + f_3(\eta) q_3$$

$$\beta = q_4$$

where z is displacement perpendicular to plane of fin

α is line-of-flight incidence of fin

β is rudder incidence relative to fin

η is a non-dimensional spanwise variable

and $f_1 = \eta^2$ at an uncoupled frequency of 9.2 c.p.s.

$$\left.\begin{array}{l} f_2 = \eta^2 \\ f_3 = \eta^3 \end{array}\right\} \text{fundamental coupled frequency 13.5 c.p.s.}$$

The calculated fin flutter speed is 1028 knots at a frequency of 11 c.p.s. The rudder degree of freedom has a destabilizing effect although not very pronounced. For a rudder rotation frequency of 10 c.p.s. the flutter speed is 922 knots.

8.2 Aircraft C

Quaternary calculations were made on this fin. The degrees of freedom were: fin parabolic bending, fin linear torsion about 0.45-chord line, rudder rotation, rudder linear torsion (zero twist at its base).

i.e.

$$z \text{ (flexural axis)} = c_r \eta^2 q_1$$

$$\alpha_f = \eta q_2$$

$$\beta = q_3 + \eta q_4$$

where α_f is the incidence perpendicular to the flexural axis. The two coupled frequencies associated with the fin modes were 5.2 and 26 c.p.s.; the frequencies of the rudder rotation and rudder torsion modes were left as variables. Curves of flutter speed against rudder torsion frequency at constant rudder rotation frequencies are given in fig.20. For a rudder rotation frequency of 12.3 c.p.s. - as shown in fig.20 - there is a low frequency type of flutter only. At the higher rotation frequencies, 18.0 and 24.5 c.p.s., there is a high frequency branch as well as the low frequency branch. Any increase in rotation frequency has the effect of raising the lower frequency curve and pushing the nose of the high frequency curve to the right. Thus, for a given torsion frequency, gain - in terms of flutter speed - in the lower frequency type as a result of increasing the rotation frequency, is restricted by the encroaching nose of the high frequency flutter curve. Further gain may however be accomplished by increasing the elevator torsion frequency.

8.3 Aircraft E

This aircraft has two fins, one at each wing tip. Senary flutter calculations were made involving the following modes: wing parabolic bending (2.77 c.p.s.), fin parabolic bending, parabolic torsion about 0.45-chord line, cubic torsion about same chord line, rudder rotation, rudder torsion (zero twist at its base). The assumed fin and rudder displacements in the fin modes were:-

$$z \text{ (flexural axis)} = c_r f_2(\eta) q_2$$

$$\alpha_f = f_3(\eta) q_3 + f_4(\eta) q_4$$

$$\beta = q_5 + f_6(\eta) q_6$$

where α_f is incidence perpendicular to the flexural axis

and $f_2 = \eta^2$ at an uncoupled frequency of 10.2 c.p.s.

$$\left.\begin{aligned} f_3 &= \eta^2 \\ f_4 &= \eta^3 \end{aligned}\right\} \text{ fundamental coupled frequency 15.7 c.p.s.}$$

$f_6 = \eta$ frequency varied.

Curves of flutter speed against the rudder torsion frequency for various rudder rotation frequencies are given in fig.21.

9 Comparison of the flutter characteristics of the three fins

Flutter characteristics of the fins and related data are given below for comparison.

Item	Fin A	Fin C	Fin E
Flutter speed in knots	1028	894	756
Flutter frequency in c.p.s.	11.0	14.0	12.8
Frequency parameter	0.76	0.67	0.53
Skin thickness in ins. (in torsion	0.060(steel)	0.035(steel)	0.11(dural)
(in bending	"	0.042	"
Thickness/chord ratio	3	4	4
Span in ft	16.0	13.6	13.1
Chord at 0.7 span in ft	18.98	11.42	8.36
Distance of flexural axis aft of l.e. (in chords)	0.45	0.45	0.45
Distance of inertia axis aft of l.e. (in chords)	0.57	0.45	0.5

10 Concluding remarks

Wing, foreplane and fin flutter calculations, and aileron reversal calculations, have been described; and it is felt that this record of the results will serve to indicate the magnitude of the aeroelastic problems to be expected on future supersonic designs. These results, on which the tender assessments as regards aeroelasticity were based, were then used to compare on an aeroelastic basis the types of planform chosen by the firms. To do this, variables from tender to tender such as thickness/chord ratio and skin thickness were eliminated by scaling the flutter speeds to correspond to the same values of thickness/chord ratio and skin thickness. Wing B was not subjected to this treatment because of its essentially different form of construction. It has, however, very desirable flutter characteristics. Of the four that were compared, the planform of wing C appears to be by far the best in terms of flutter speed per unit skin mass. The other three, wings A, D and E, have very comparable flutter characteristics. On aileron reversal the planform of C was still ahead, but the planform of wing A was better than that of E, possibly as a result of its lack of structural sweep. No aileron reversal calculations were made on aircraft D. It was not possible to say with any certainty whether aileron reversal or flutter was the more critical design case: on aircraft A flutter appeared to be the more critical; on aircraft E it seemed likely to be aileron reversal. On aircraft C aileron reversal requirements - in terms of skin thickness - were the greater; but both cases were far from critical.

The results of the foreplane flutter calculations are of particular interest because of the unconventional canard layouts. The effects of the control frequencies and fuselage modes were investigated and the results presented in graphical form. It was seen that divergence, primarily between the fuselage flexure and foreplane rotation modes, is a possibility if the foreplane control stiffness is low. The need to include body freedoms of pitch and vertical translation in the symmetric flutter calculations was also noted. On the three foreplanes where both symmetric and antisymmetric flutter calculations were made, the symmetric flutter speed was lower than the antisymmetric when the foreplane rotation frequency was well above the foreplane bending frequency and when the elevator was, in effect, locked. This was due, in part, to the stabilizing effect of the fuselage torsion mode at certain frequencies.

The value of all the results is limited by the simple approach that has been adopted throughout.

Acknowledgement

The basic work reported in this paper was carried out by the Staff of Structures Dept. and acknowledgements are due to Messrs. E.G. Broadbent, A.D.N. Smith, Ll.T. Niblett and Miss D.M. Seal and Miss M.P. Williams.

REFERENCES

No.	Author	Title, etc.
1	I.T. Minhinnick	A symposium on the flutter problem in aircraft design (Edited by H. Templeton and G.R. Brooke), paper 4. Unpublished M.O.A. Report.
2	D.L. Woodcock	Aerodynamic derivatives for a delta wing oscillating in elastic modes. Current Paper No.170, July 1953.

Printed in England for Her Majesty's Stationery Office by the Royal Aircraft Establishment, Farnborough. W.T.60.K.4.

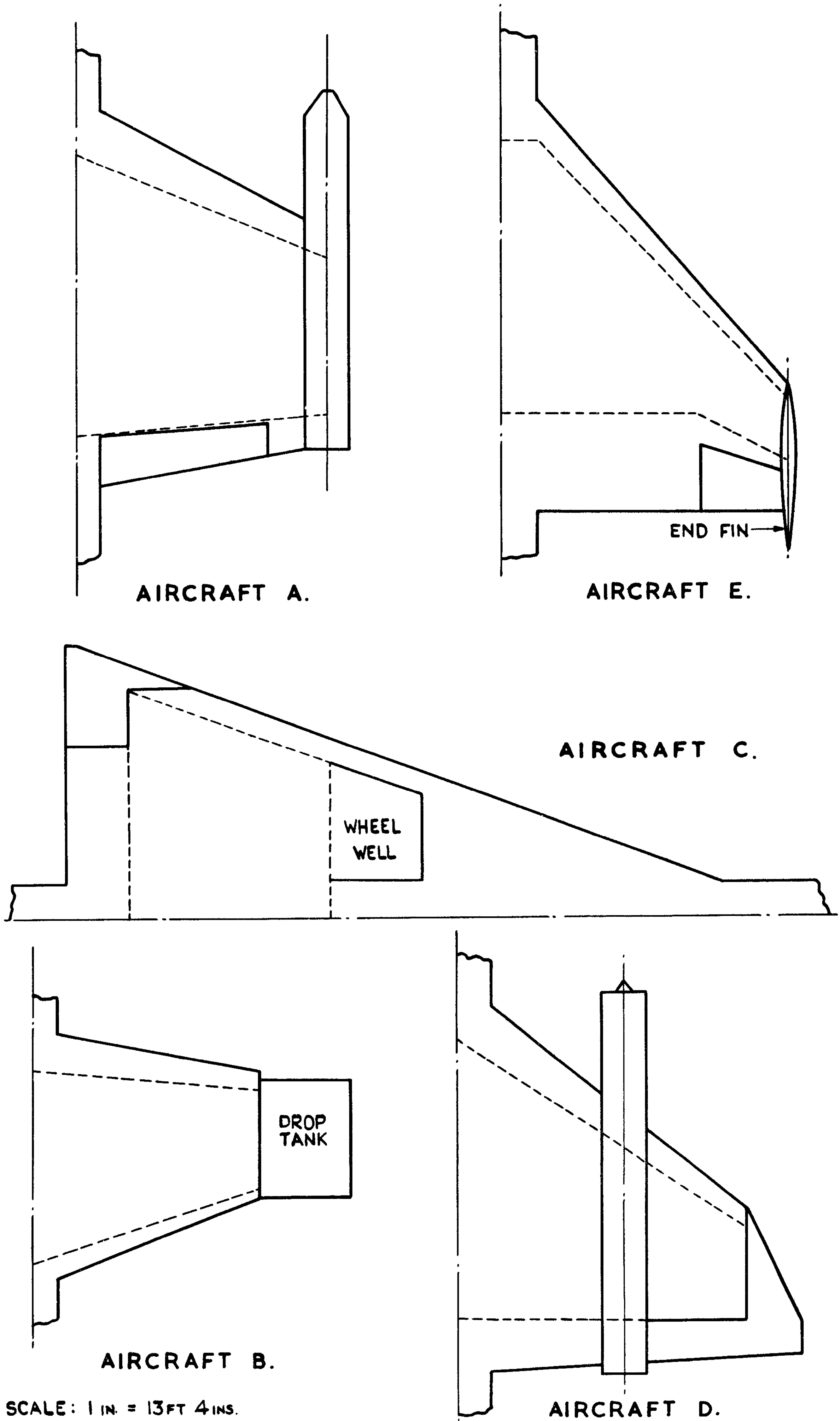

FIG. 1. WING PLANFORMS.

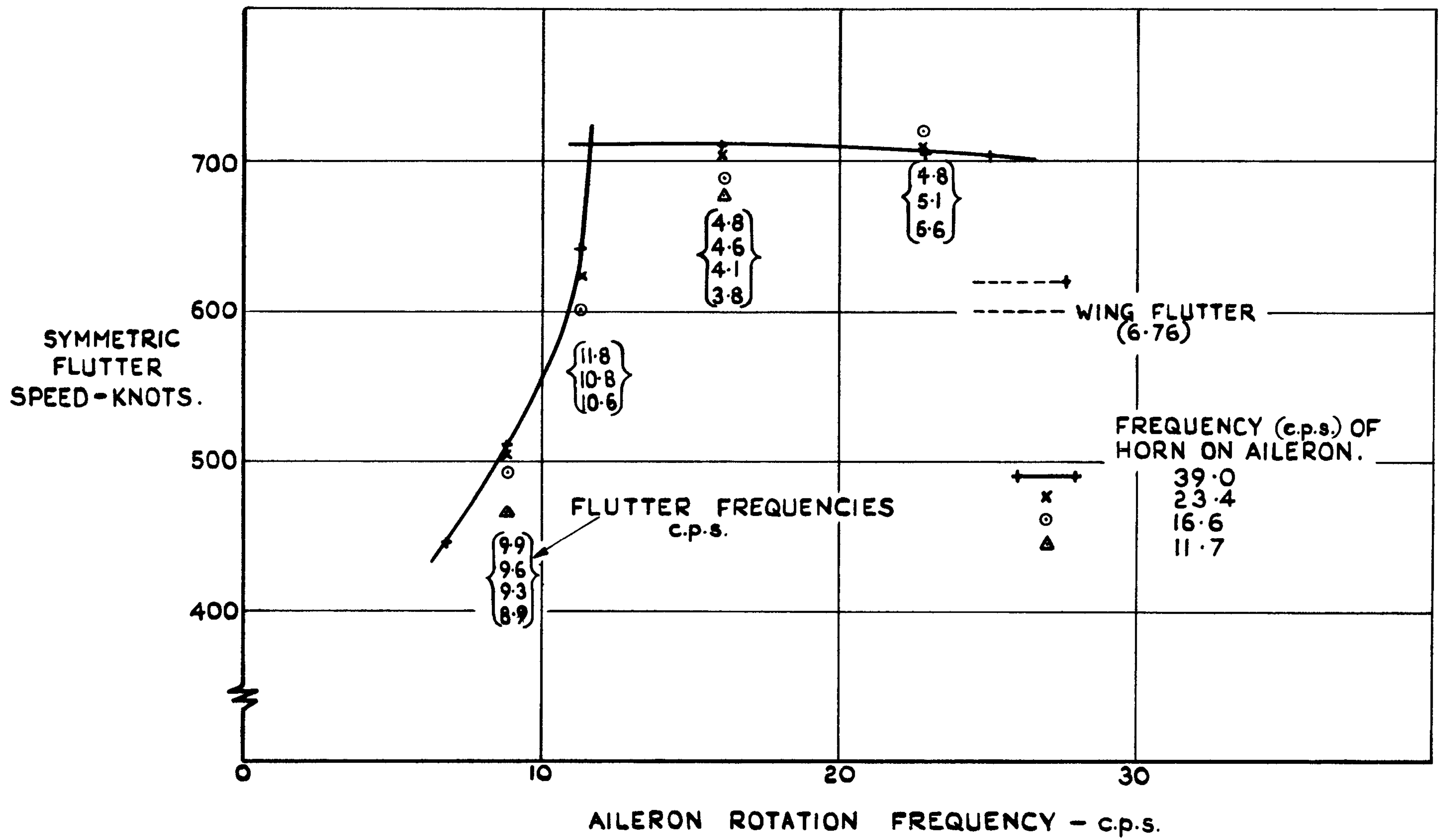

FIG. 2. EFFECT OF AILERON AND HORN ROTATION FREQUENCIES ON SYMMETRIC FLUTTER-AIRCRAFT D.

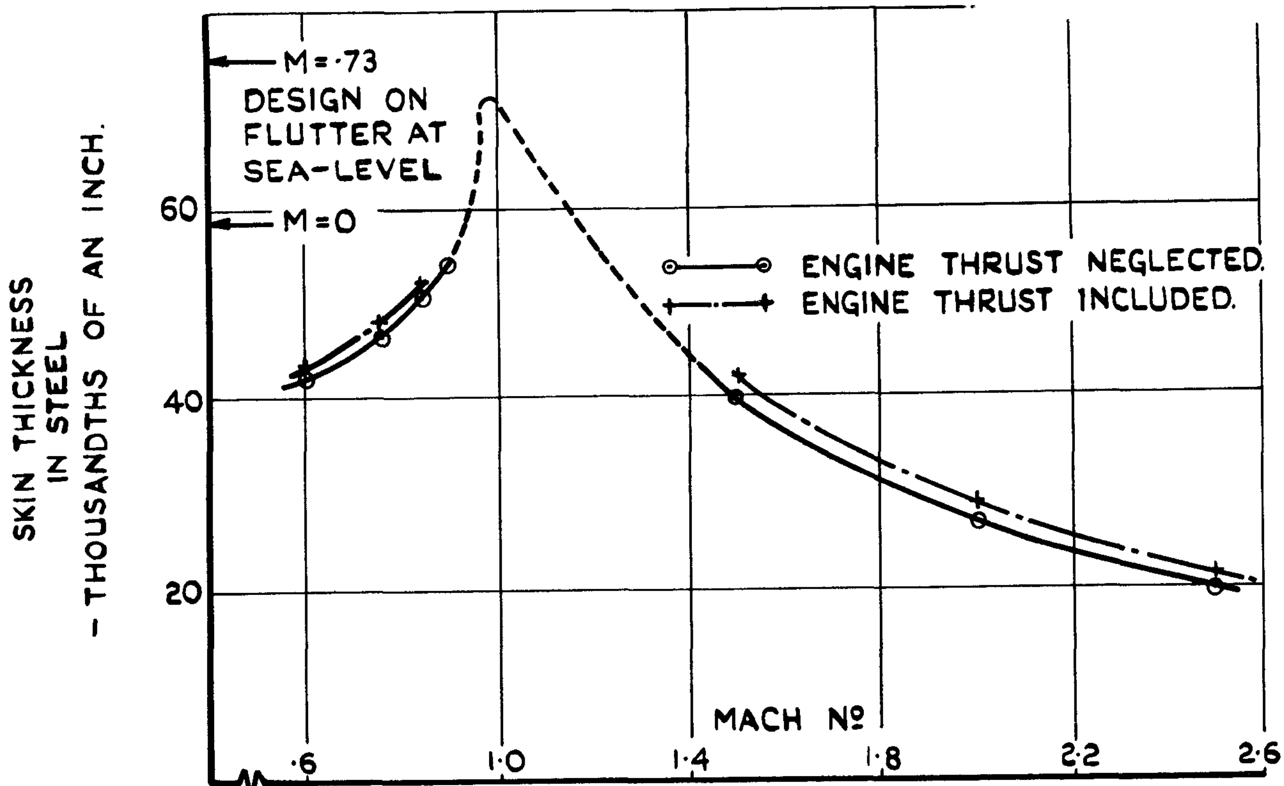

FIG. 3. VARIATION OF REQUIRED SKIN THICKNESS WITH MACH Nº FOR A REVERSAL SPEED OF 559 KNOTS E.A.S.-AIRCRAFT A.

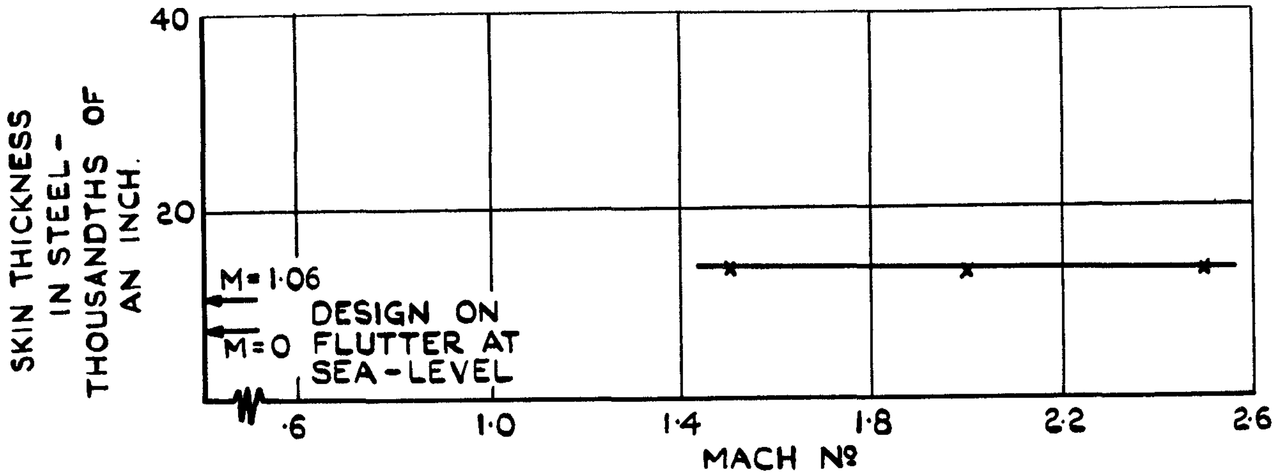

FIG. 4. VARIATION OF REQUIRED SKIN THICKNESS WITH MACH Nº FOR A REVERSAL SPEED OF 805 KNOTS E.A.S.-AIRCRAFT C.

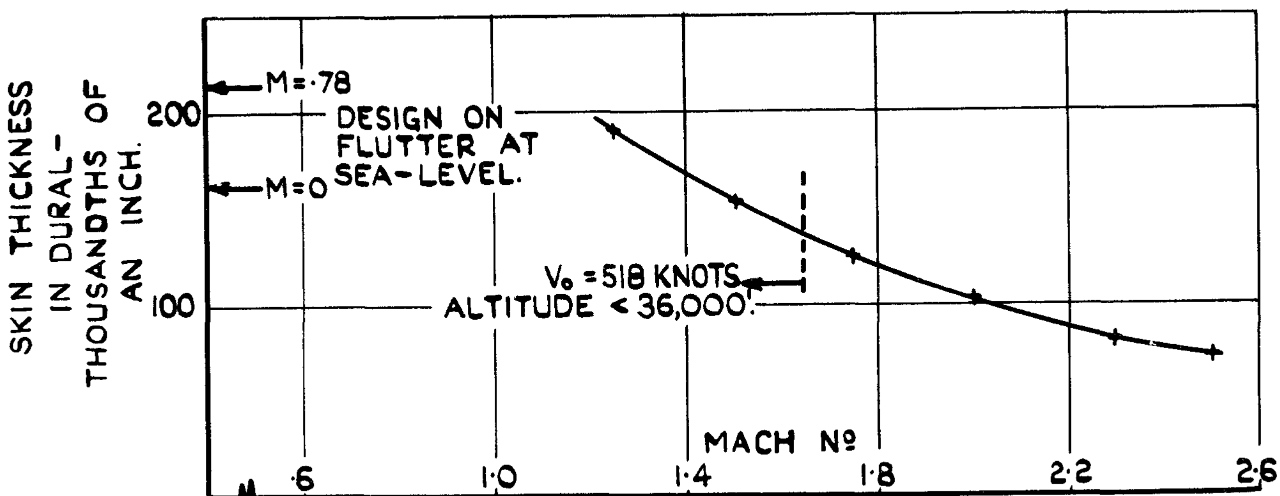

FIG. 5. VARIATION OF REQUIRED SKIN THICKNESS WITH MACH Nº FOR A REVERSAL SPEED OF 595·7 KNOTS E.A.S.-AIRCRAFT E.

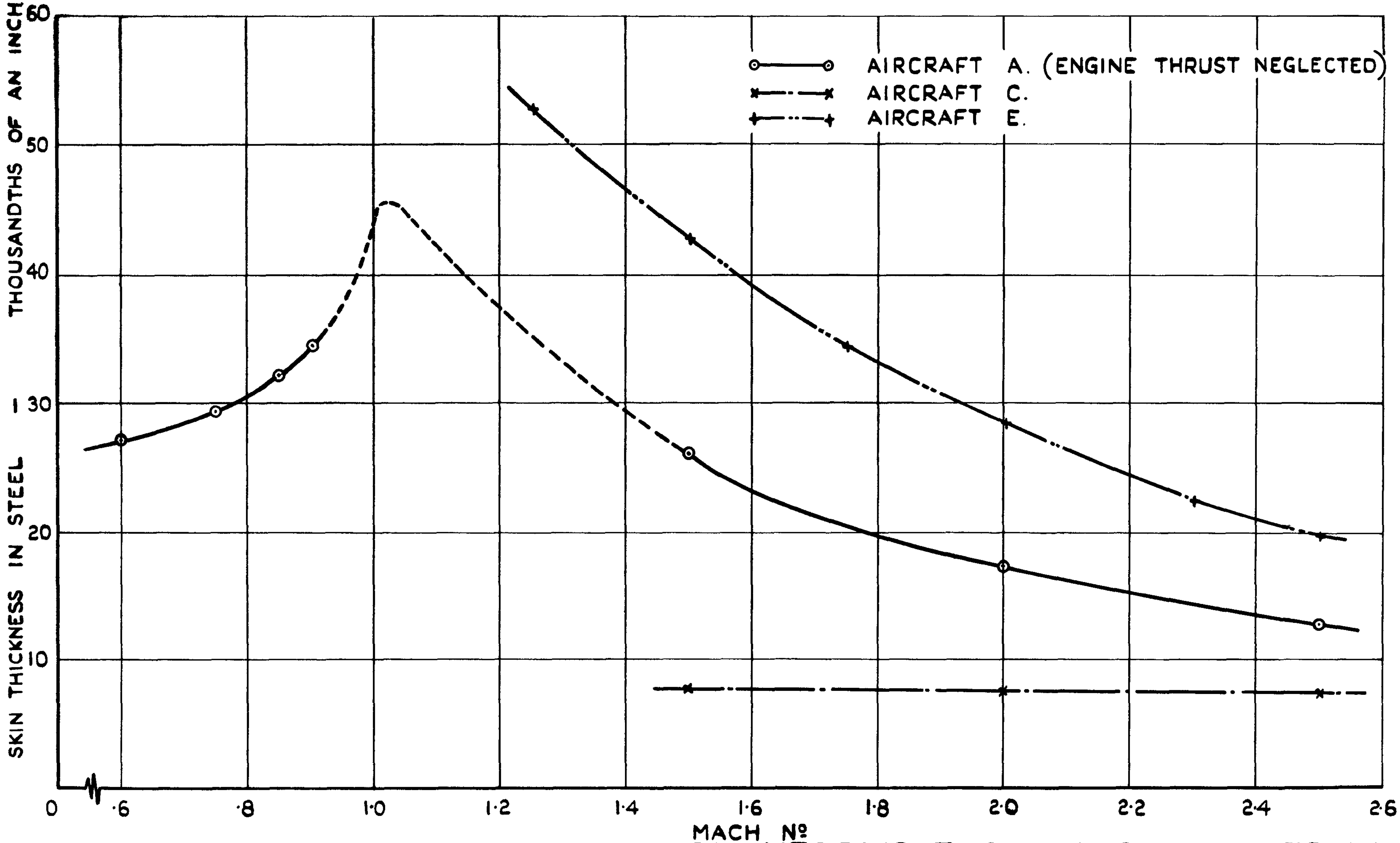

FIG. 6. COMPARISON OF THE THREE PLANFORMS, EACH WING ASSUMED TO BE 4% THICK AND OF STEEL CONSTRUCTION & HAVING A REVERSAL SPEED OF 600KTS. E.A.S.

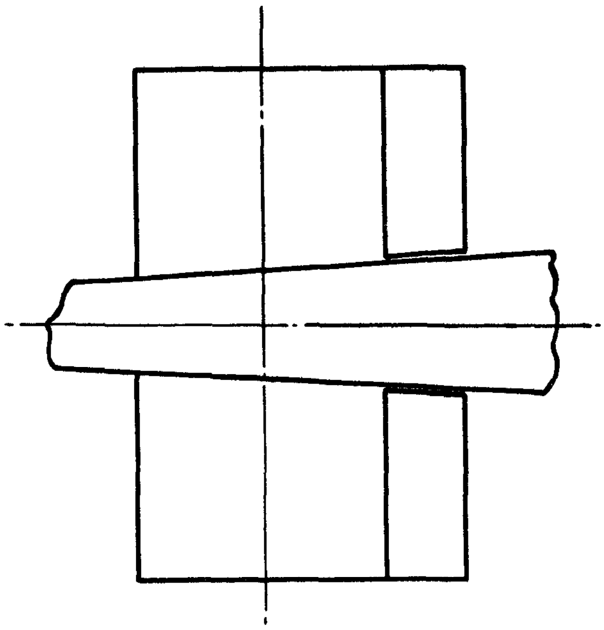

AIRCRAFT A

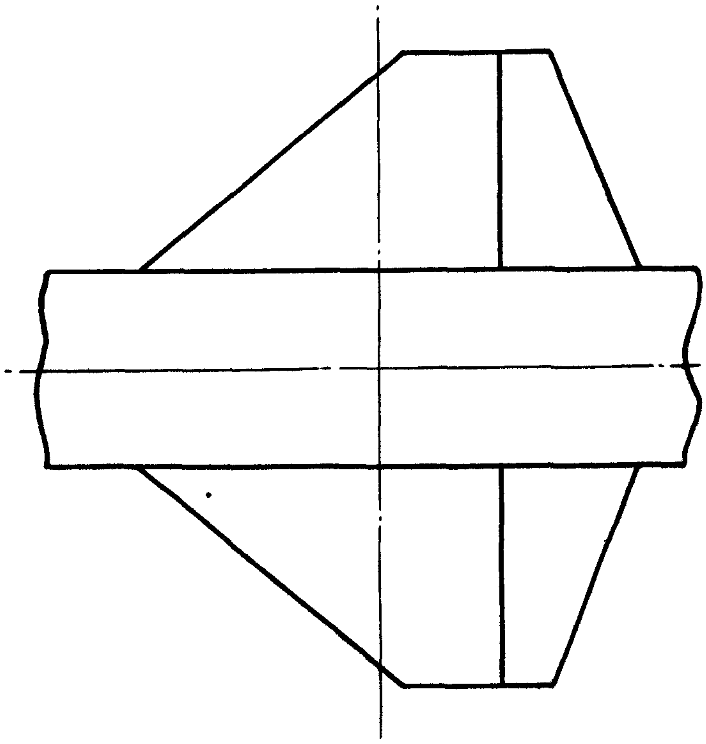

AIRCRAFT E

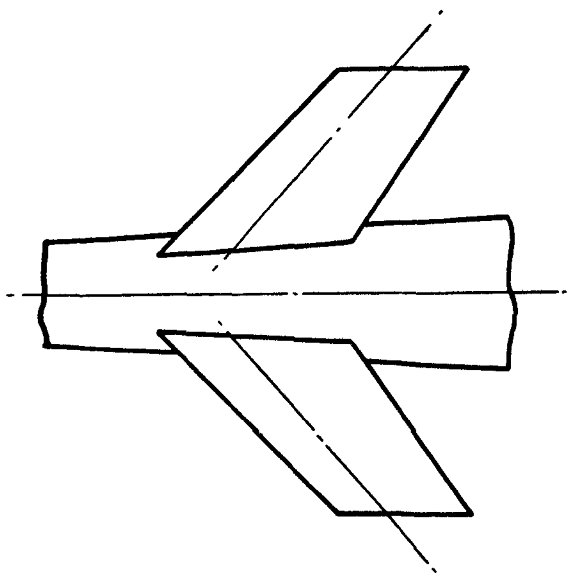

AIRCRAFT B

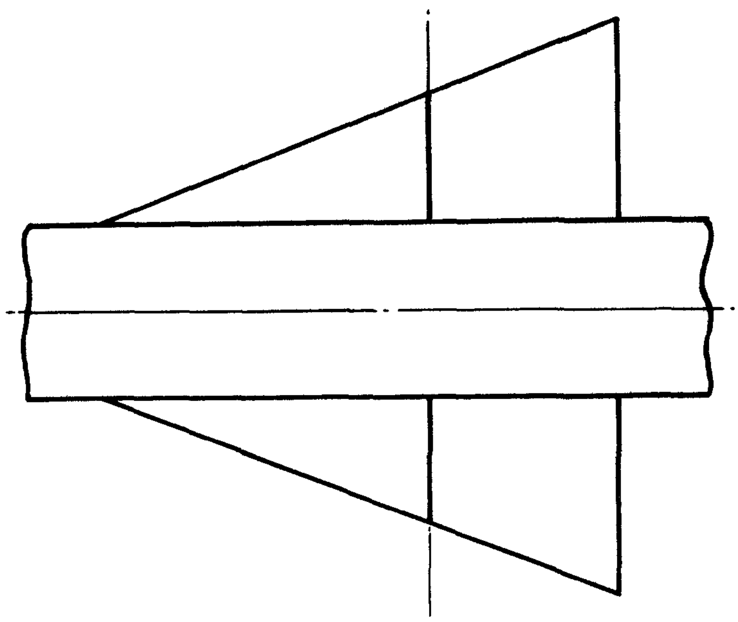

AIRCRAFT C

SCALE: 1 INCH = 8 FT.

FIG. 7. FOREPLANE PLANFORMS

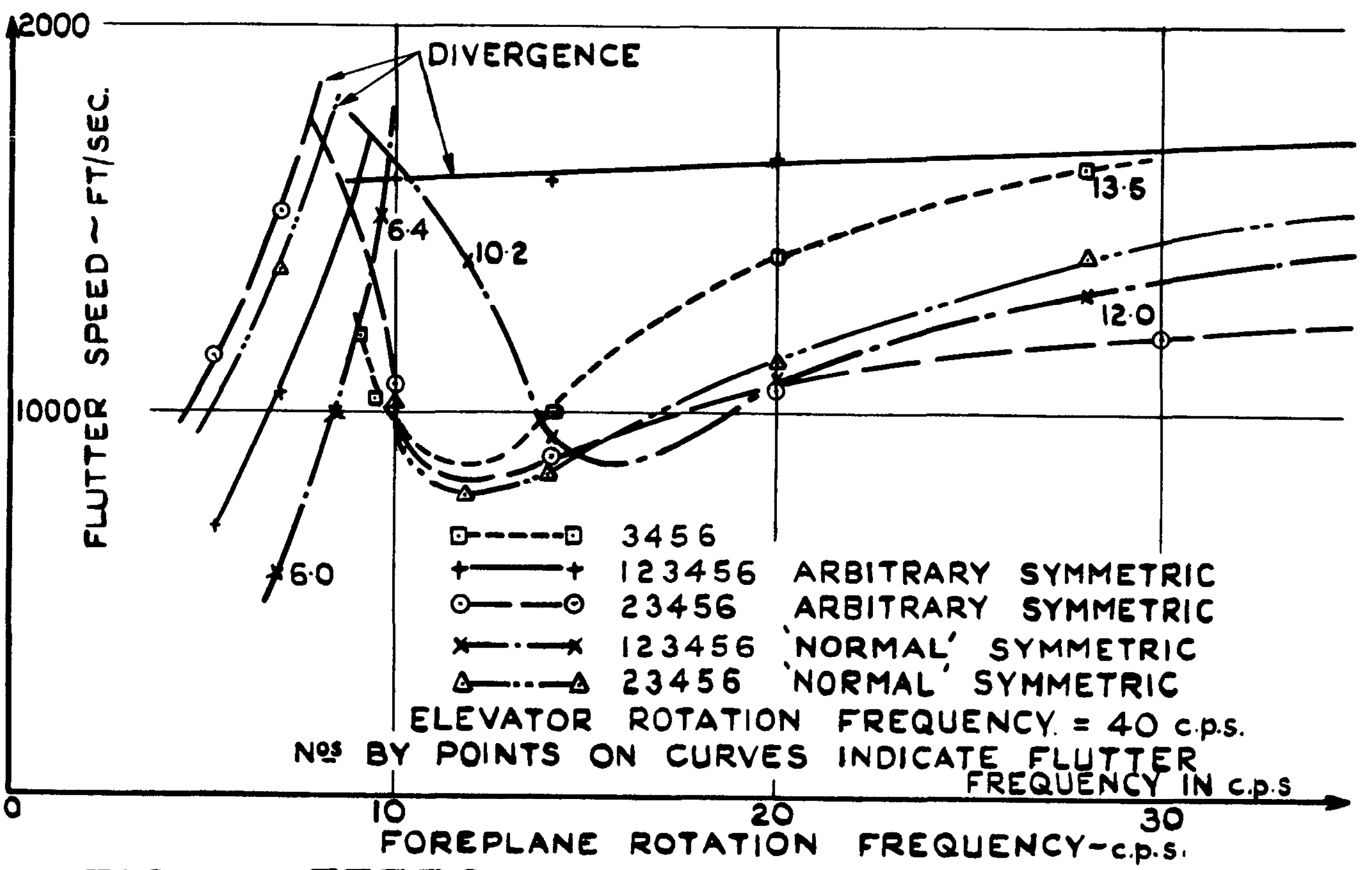

FIG. 8. EFFECT OF FOREPLANE ROTATION FREQUENCY AND FUSELAGE MODES ON SYMMETRIC FLUTTER-AIRCRAFT A.

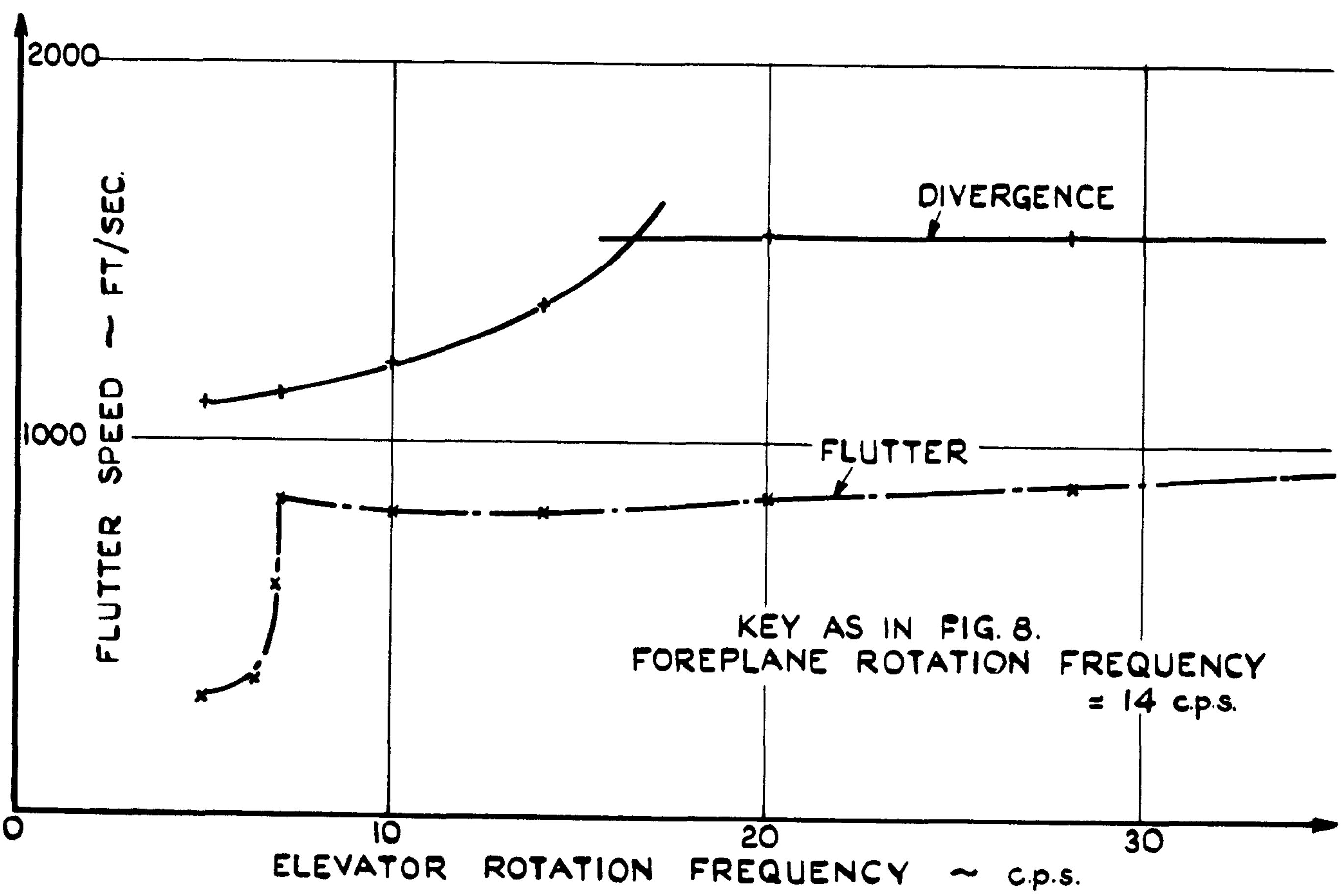

FIG. 9. SYMMETRIC FLUTTER SPEED AGAINST ELEVATOR ROTATION FREQUENCY-AIRCRAFT A

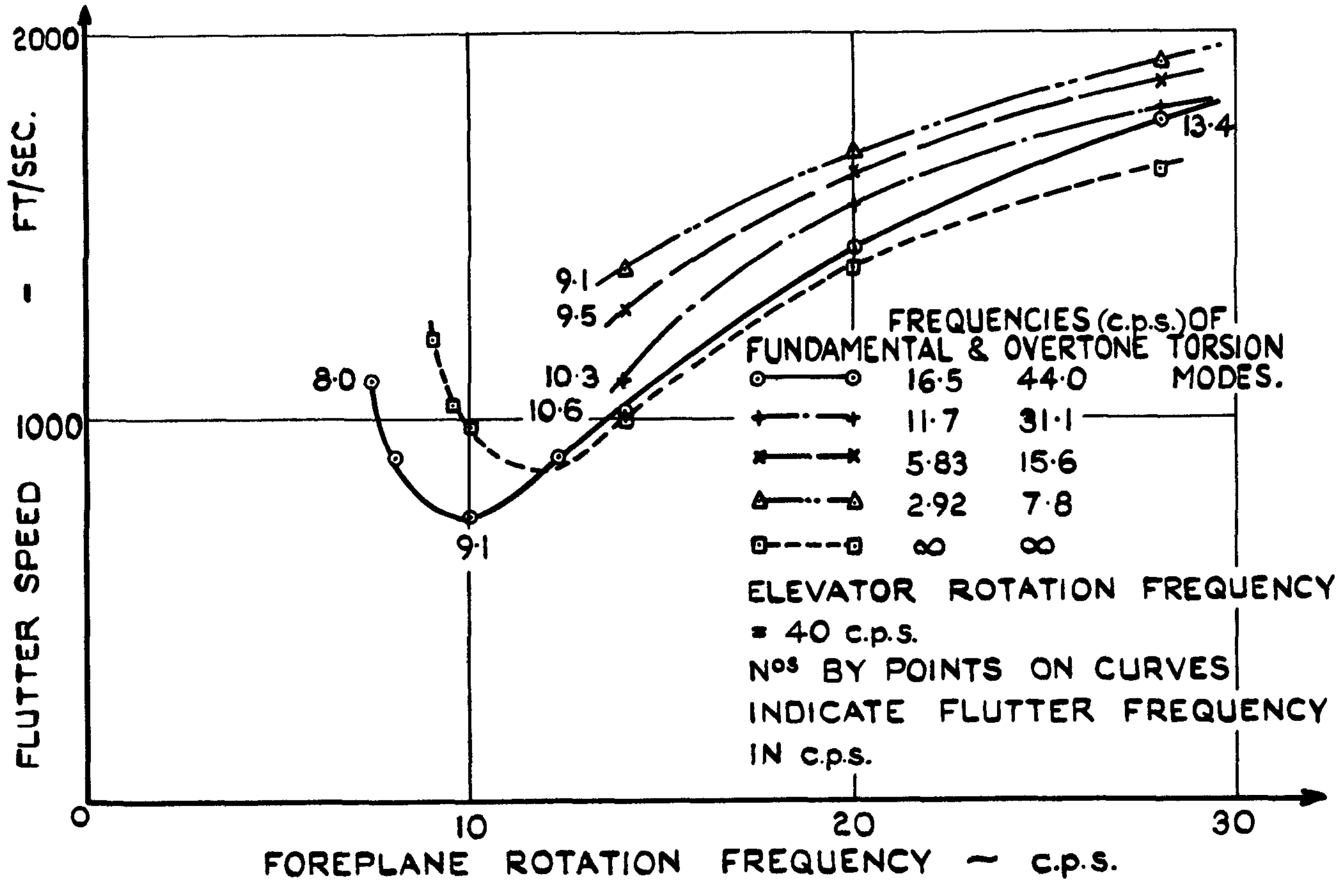

FIG. 10. EFFECT OF FOREPLANE ROTATION AND FUSELAGE TORSION FREQUENCIES ON ANTISYMMETRIC FLUTTER—AIRCRAFT A.

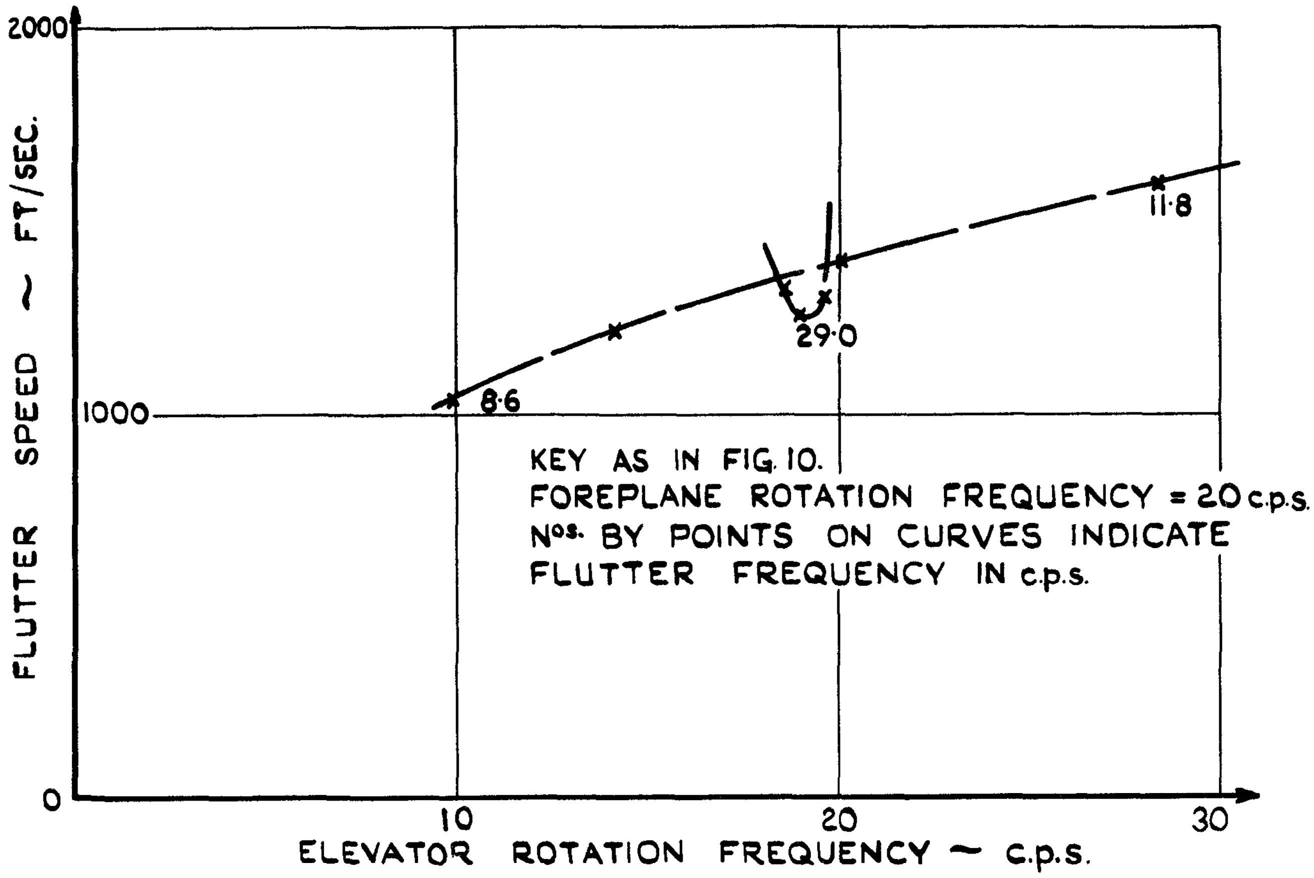

FIG. 11. ANTISYMMETRIC FLUTTER SPEED AGAINST ELEVATOR ROTATION FREQUENCY-AIRCRAFT A.

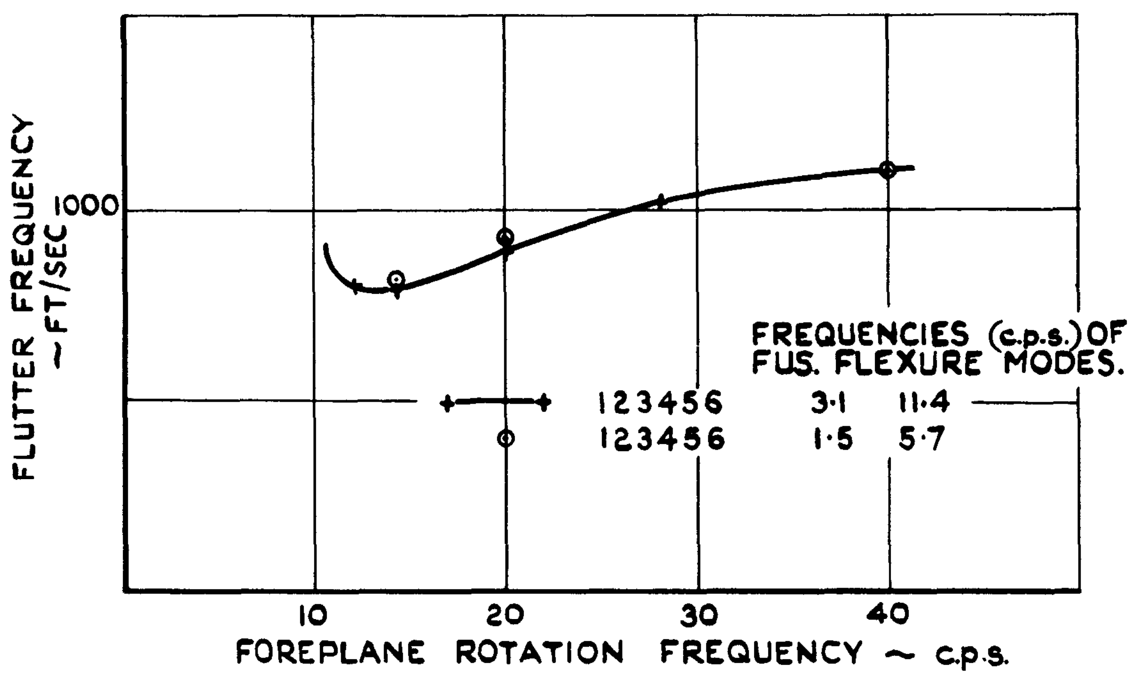

FIG. 12. EFFECT OF FOREPLANE ROTATION AND FUSELAGE FLEXURE FREQUENCIES ON SYMMETRIC FLUTTER—AIRCRAFT B.

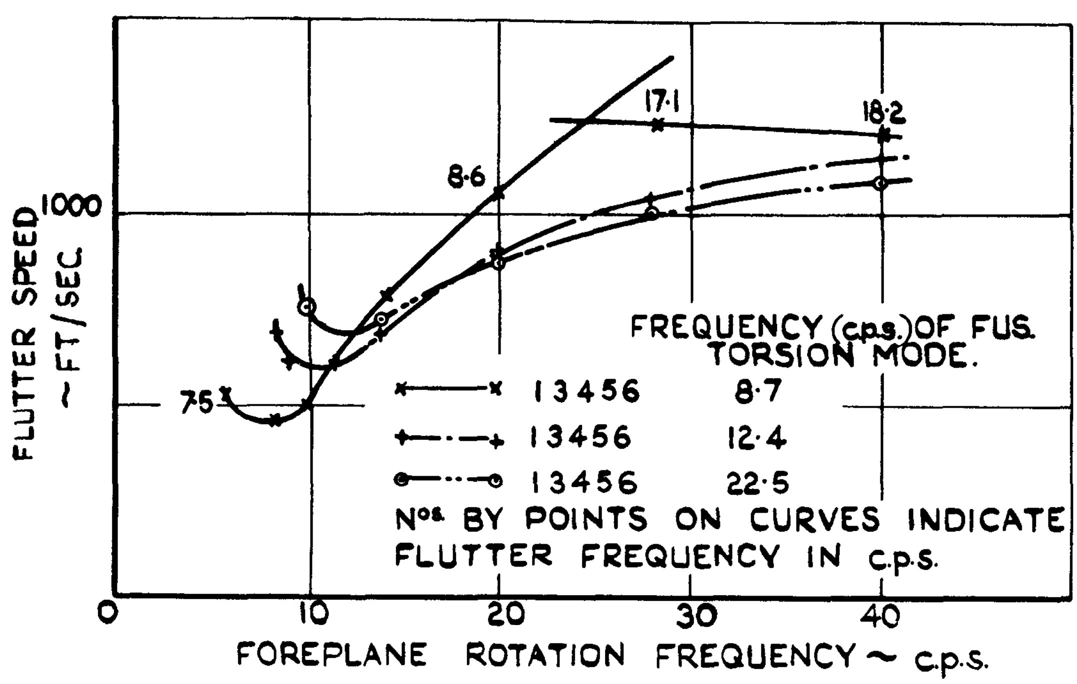

FIG. 13. EFFECT OF FOREPLANE ROTATION AND FUSELAGE TORSION FREQUENCIES ON ANTISYMMETRIC FLUTTER—AIRCRAFT B.

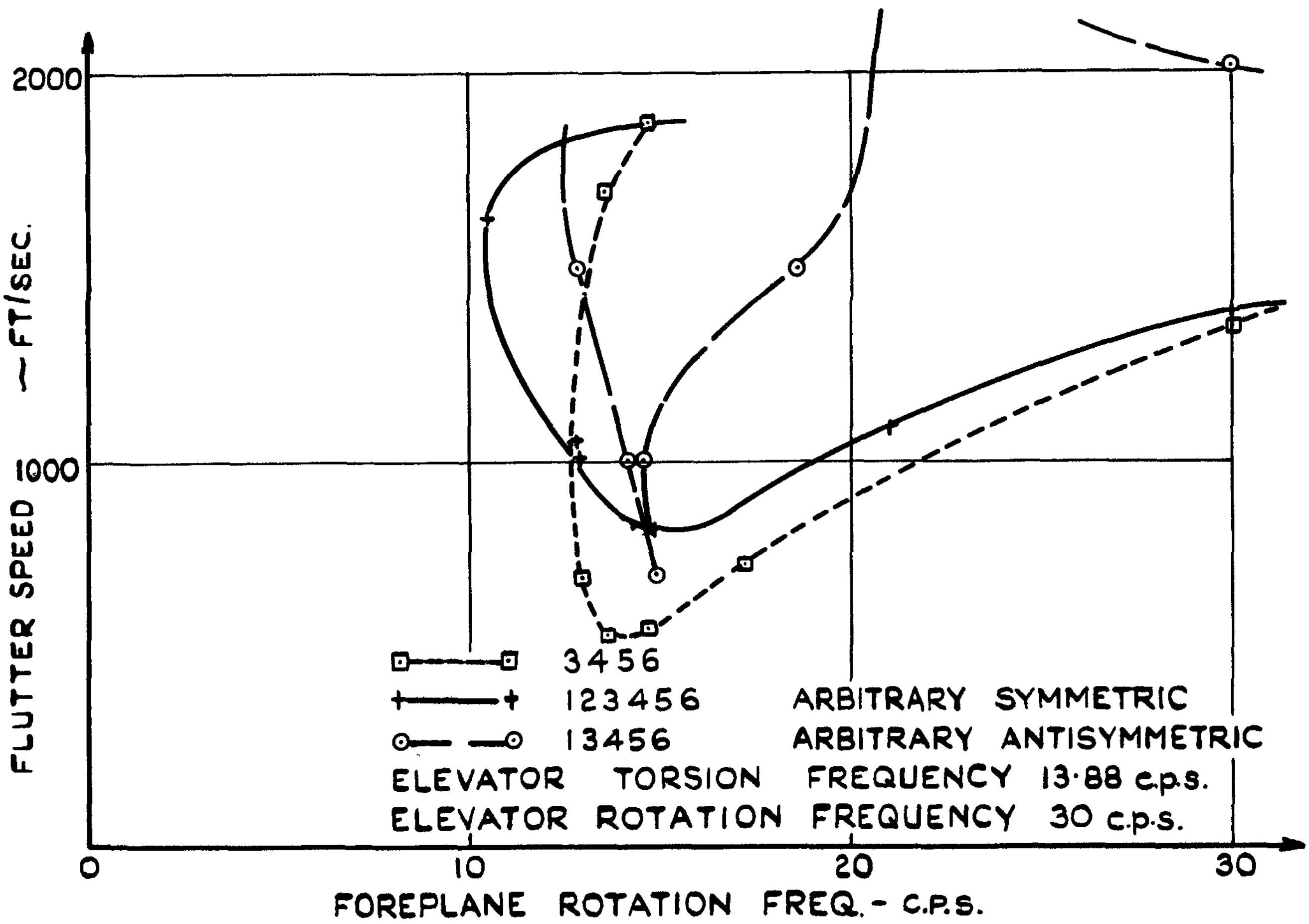

FIG. 14. EFFECT OF FOREPLANE ROTATION FREQUENCY AND FUSELAGE MODES (BOTH SYMMETRIC & ANTISYMMETRIC) ON FLUTTER - AIRCRAFT C.

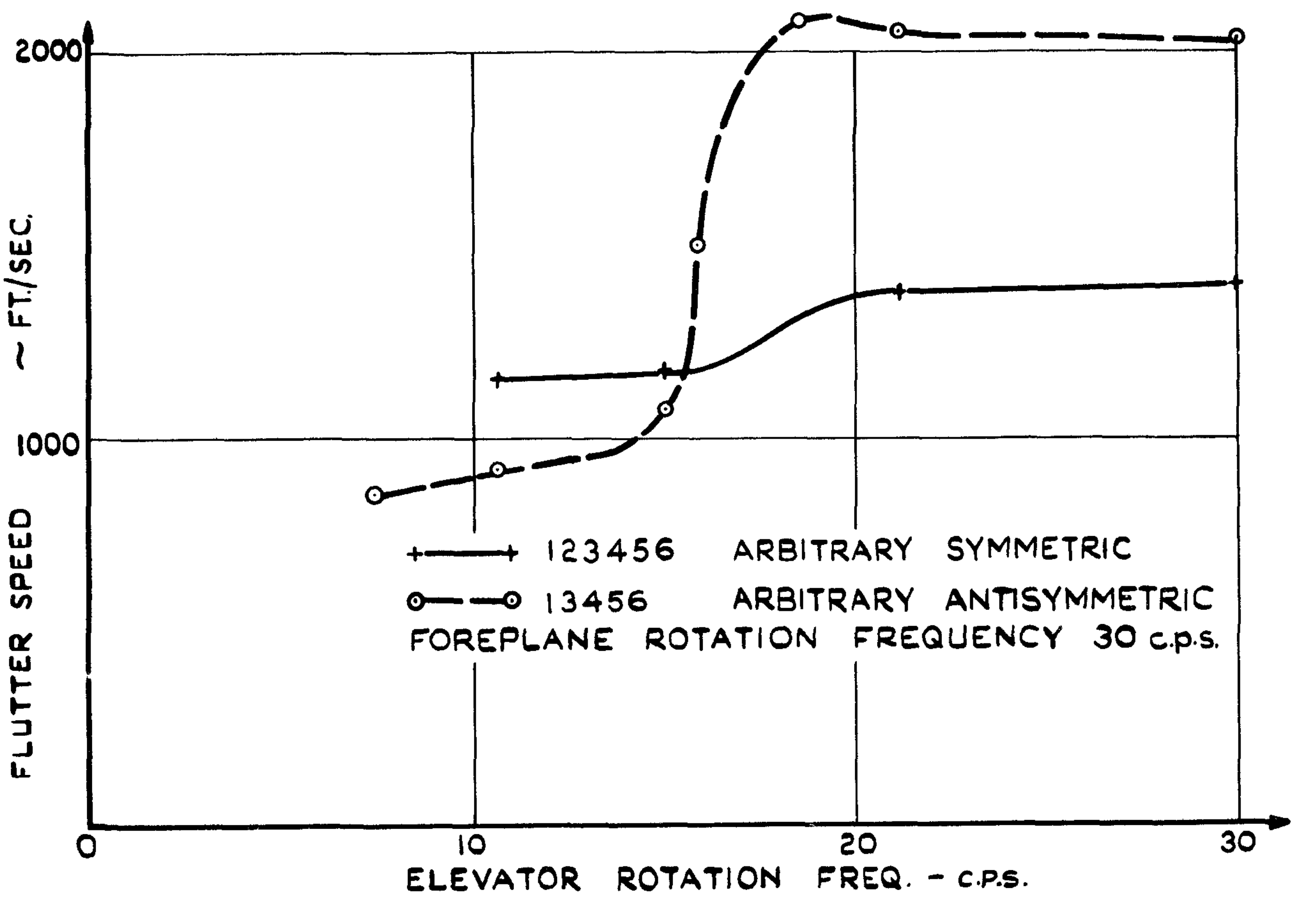

FIG. 15. SYMMETRIC FLUTTER SPEED AGAINST ELEVATOR ROTATION FREQUENCY-AIRCRAFT C.

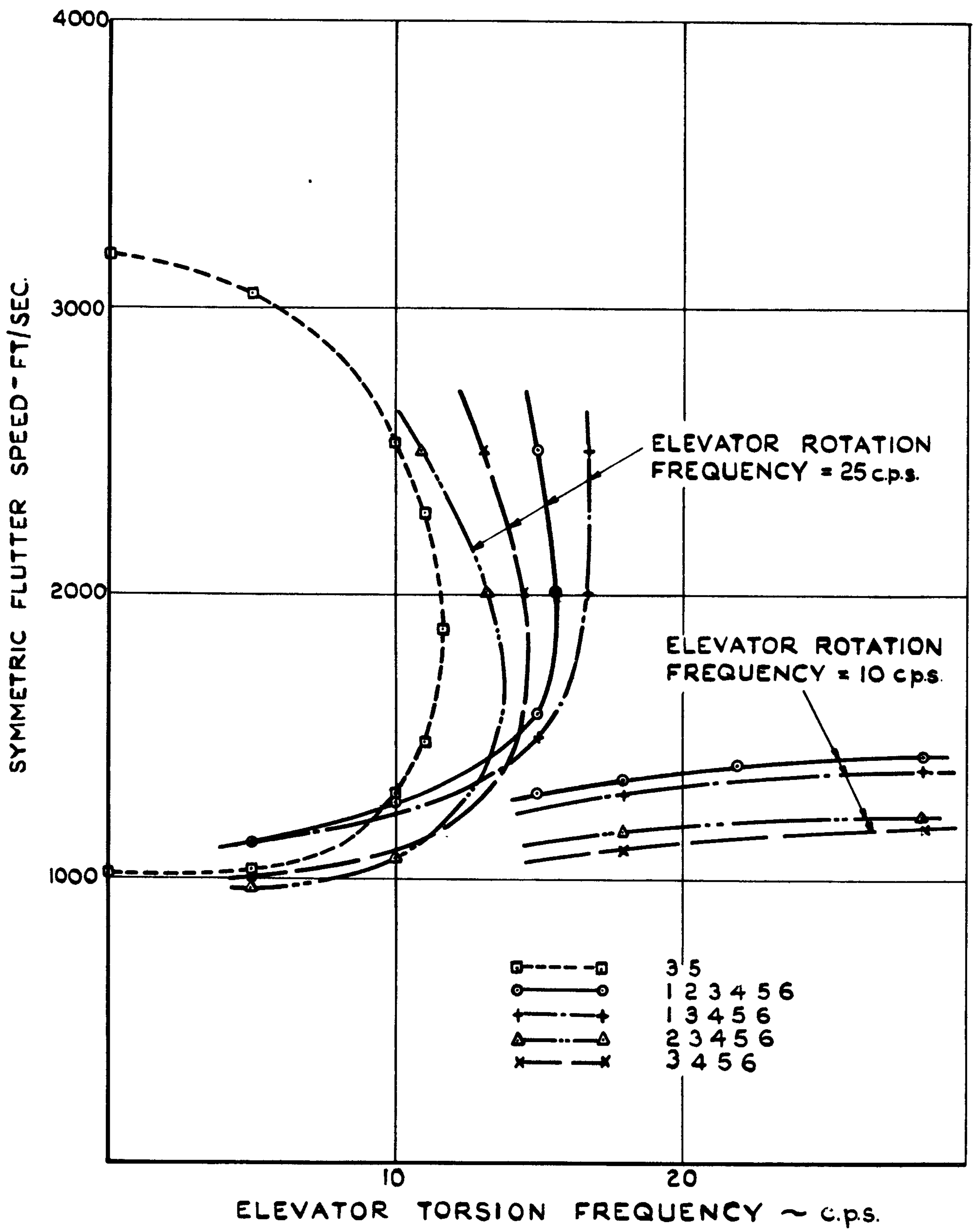

FIG. 16. SYMMETRIC FLUTTER SPEED AGAINST ELEVATOR TORSION FREQUENCY; EFFECT OF FUSELAGE BENDING MODES—AIRCRAFT C.

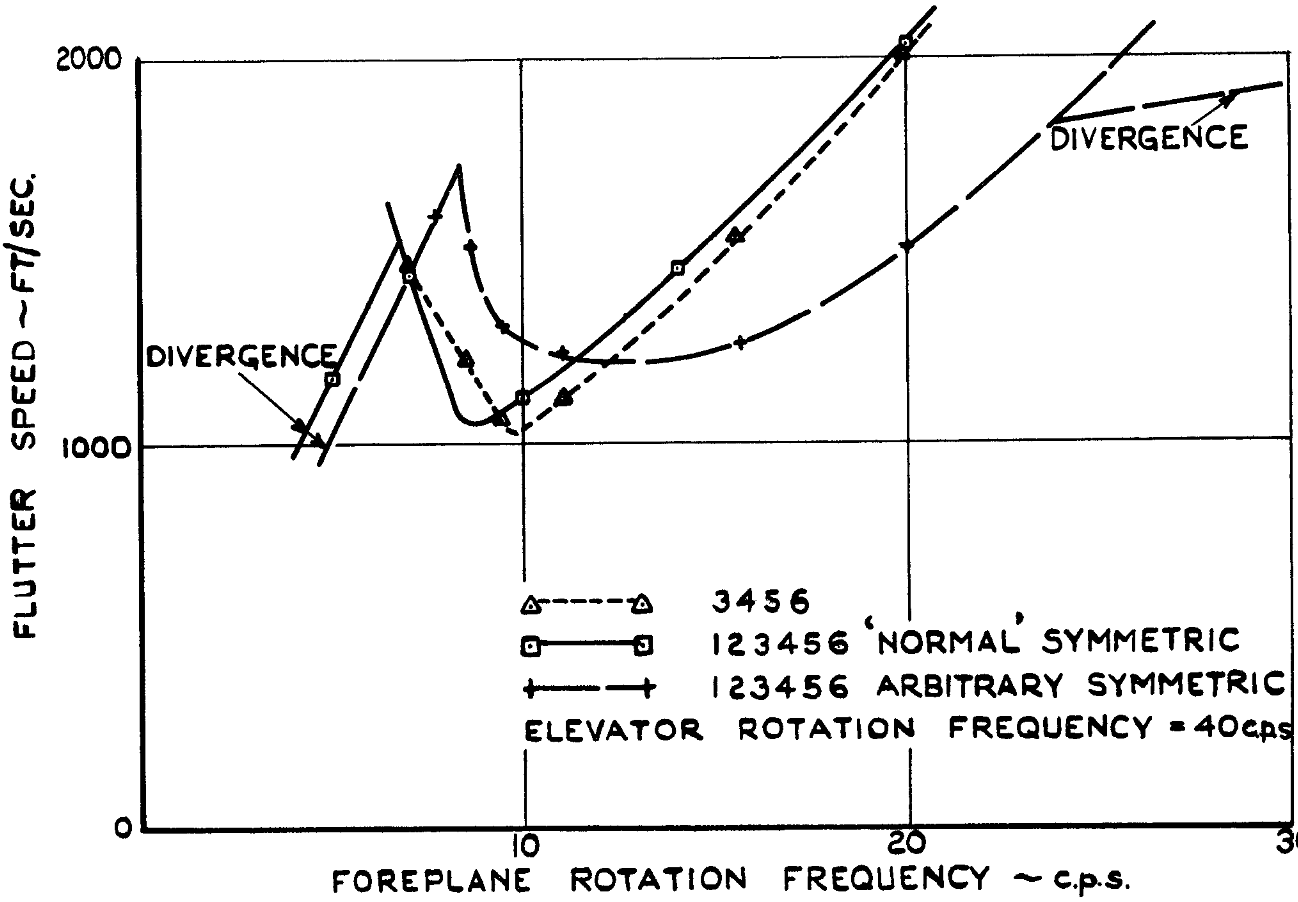

FIG. 17. EFFECT OF FOREPLANE ROTATION FREQUENCY & FUSELAGE MODES ON SYMMETRIC FLUTTER-AIRCRAFT E.

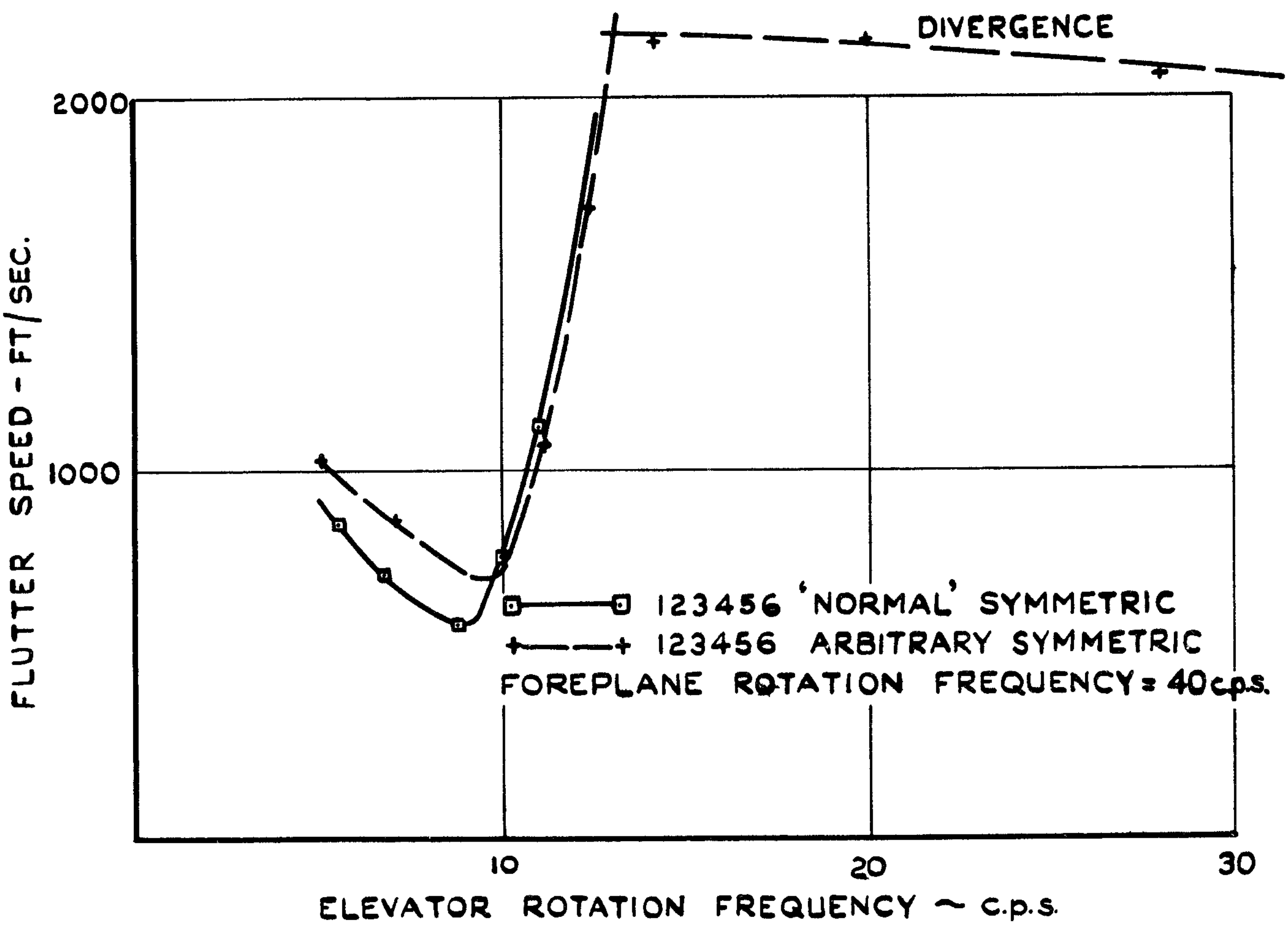

FIG. 18. SYMMETRIC FLUTTER SPEED AGAINST ELEVATOR ROTATION FREQUENCY-AIRCRAFT E.

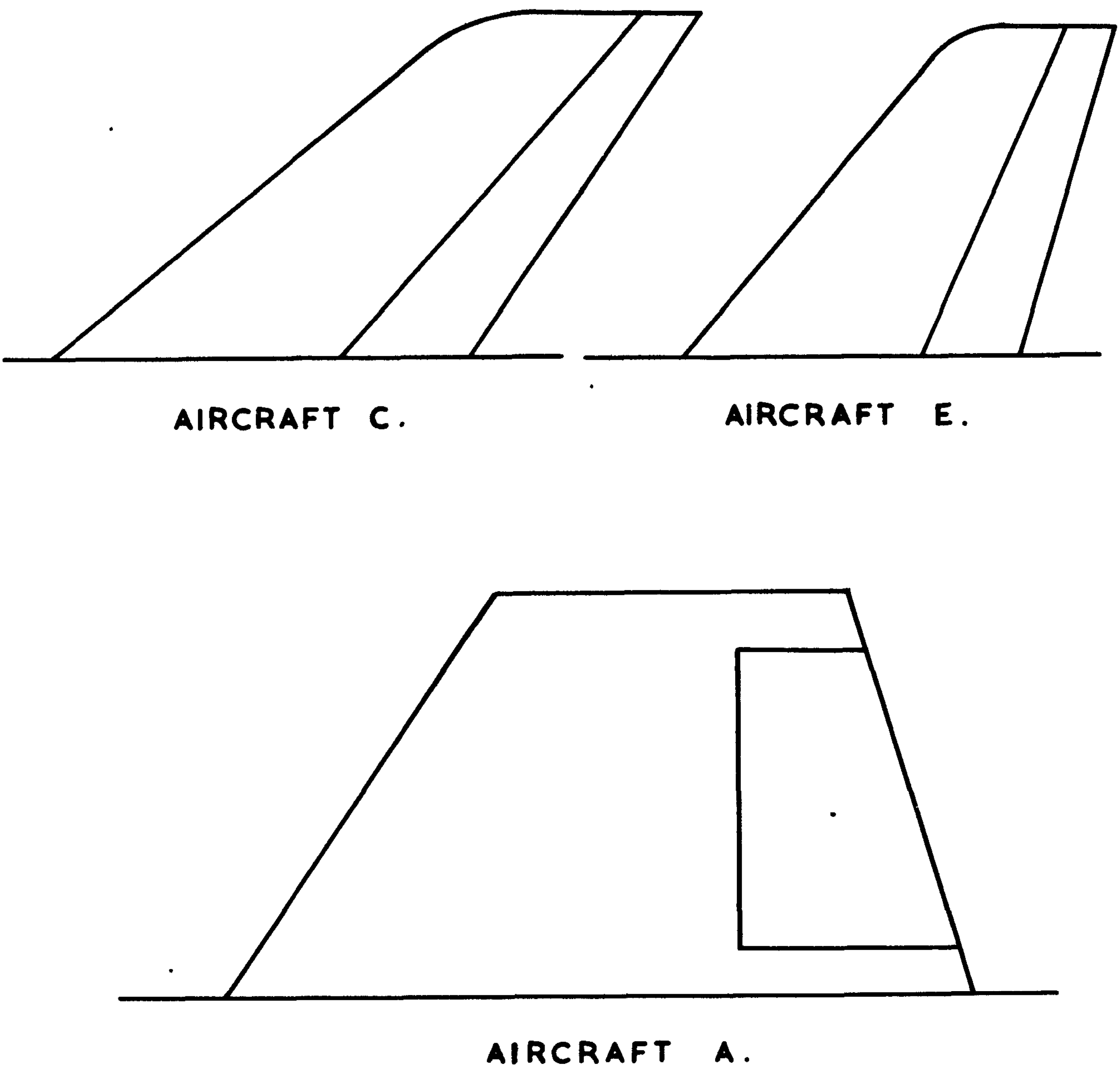

SCALE: 1 INCH = 6 FT 8 INS.

FIG. 19. FIN PLANFORMS

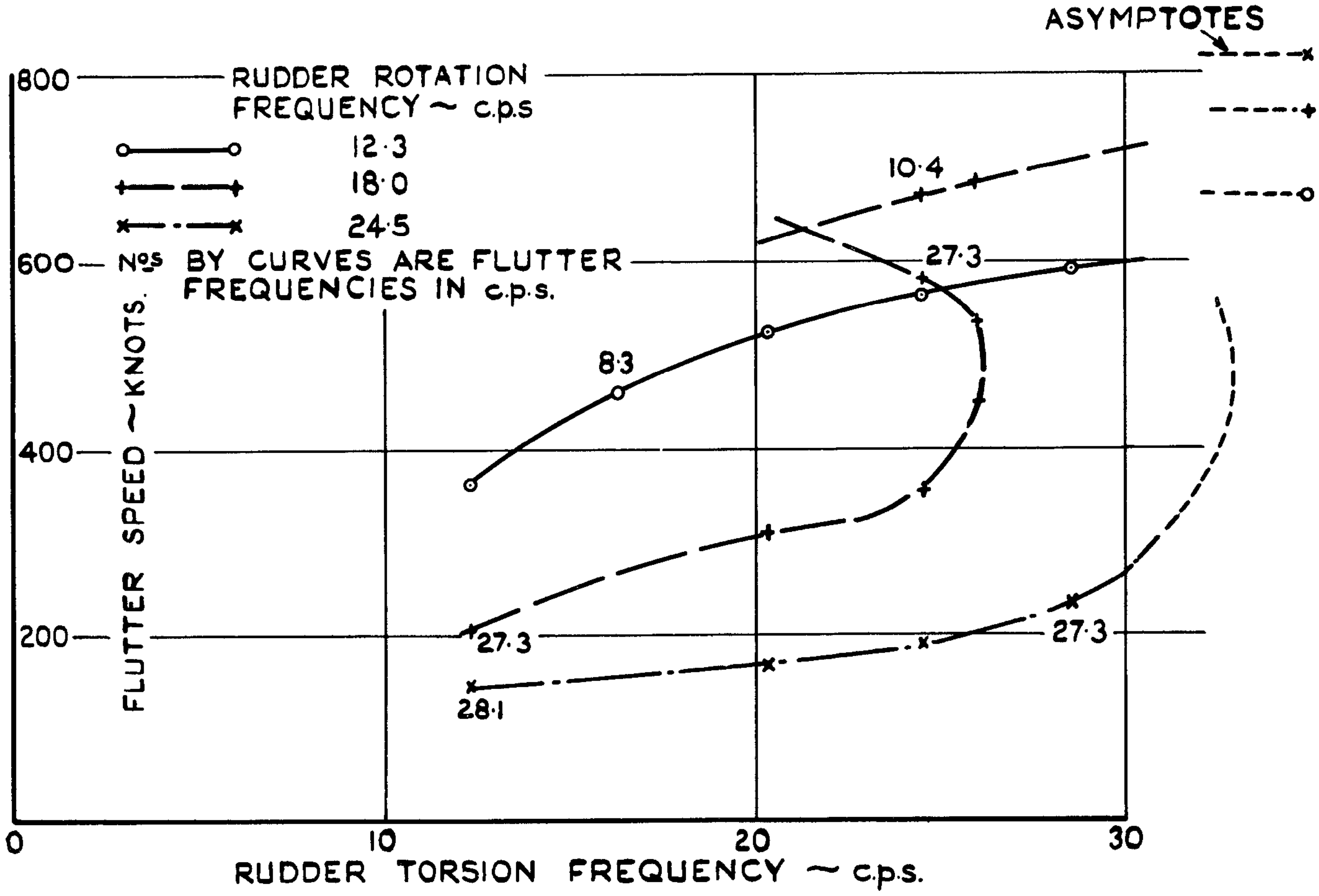

FIG. 20. EFFECT OF RUDDER TORSION ON FIN FLUTTER-AIRCRAFT C.

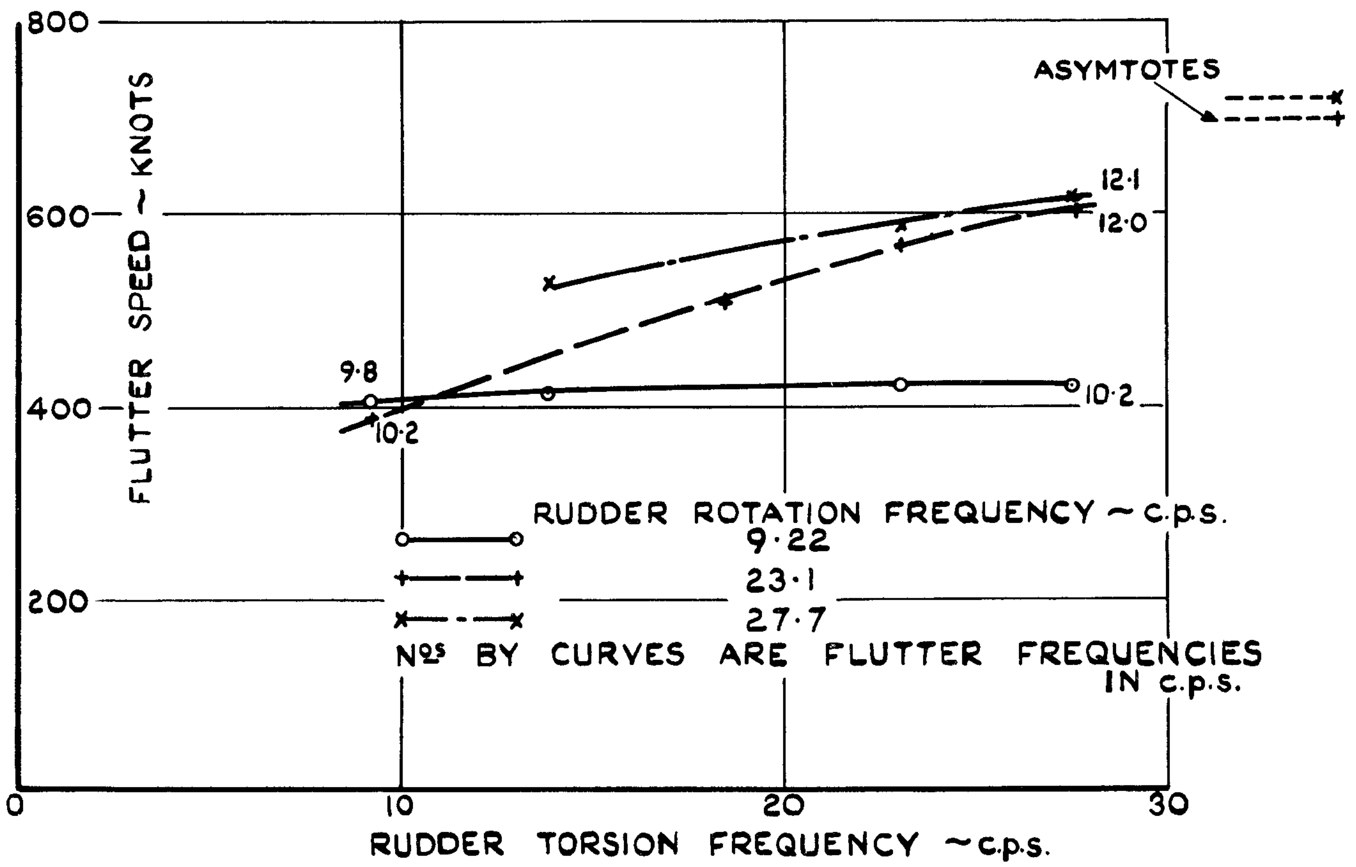

FIG. 21. EFFECT OF RUDDER TORSION ON FIN FLUTTER-AIRCRAFT E .

A.R.C. C.P. No.668
May 1957

533.6.013.42:
629.13.072.2

Moxon, D.

AEROELASTIC PROBLEMS OF HIGH SPEED AIRCRAFT

Aeroelastic calculations on a number of specific aircraft projects have recently been made to provide comparative assessments. The characteristics of the aircraft were such as to provide valuable data on the aeroelastic problems of future high speed aircraft with specific reference to wing planforms and foreplane control. The flutter, divergence and aileron reversal speeds are given for the various projects and general conclusions are drawn. Throughout the work simple arbitrary modes have been assumed and simple beam theory used in evaluating the elastic stiffnesses. Approximate three-dimensional aerodynamic derivatives have been used in most of the work, and in the flutter calculations the effect of Mach No. has been estimated only by empirical rules. The value of the results is limited by these assumptions.

A.R.C. C.P. No.668
May 1957

533.6.013.42:
629.13.072.2

Moxon, D.

AEROELASTIC PROBLEMS OF HIGH SPEED AIRCRAFT

Aeroelastic calculations on a number of specific aircraft projects have recently been made to provide comparative assessments. The characteristics of the aircraft were such as to provide valuable data on the aeroelastic problems of future high speed aircraft with specific reference to wing planforms and foreplane control. The flutter, divergence and aileron reversal speeds are given for the various projects and general conclusions are drawn. Throughout the work simple arbitrary modes have been assumed and simple beam theory used in evaluating the elastic stiffnesses. Approximate three-dimensional aerodynamic derivatives have been used in most of the work, and in the flutter calculations the effect of Mach No. has been estimated only by empirical rules. The value of the results is limited by these assumptions.

A.R.C. C.P. No.668
May 1957

533.6.013.42:
629.13.072.2

Moxon, D.

AEROELASTIC PROBLEMS OF HIGH SPEED AIRCRAFT

Aeroelastic calculations on a number of specific aircraft projects have recently been made to provide comparative assessments. The characteristics of the aircraft were such as to provide valuable data on the aeroelastic problems of future high speed aircraft with specific reference to wing planforms and foreplane control. The flutter, divergence and aileron reversal speeds are given for the various projects and general conclusions are drawn. Throughout the work simple arbitrary modes have been assumed and simple beam theory used in evaluating the elastic stiffnesses. Approximate three-dimensional aerodynamic derivatives have been used in most of the work, and in the flutter calculations the effect of Mach No. has been estimated only by empirical rules. The value of the results is limited by these assumptions.

Published by
HER MAJESTY'S STATIONERY OFFICE

To be purchased from
York House, Kingsway, London w.c.2
423 Oxford Street, London w.1
13A Castle Street, Edinburgh 2
109 St. Mary Street, Cardiff
39 King Street, Manchester 2
50 Fairfax Street, Bristol 1
35 Smallbrook, Ringway, Birmingham 5
80 Chichester Street, Belfast 1
or through any bookseller

S.O. CODE No. 23-9013-68

C.P. No. 668